

FINAL REPORT

Underwater Dynamic Classification Technology

ESTCP Project MR-201614

FEBRUARY 2018

Jonathan Miller
White River Technologies

Distribution Statement A
This document has been cleared for public release



Page Intentionally Left Blank

This report was prepared under contract to the Department of Defense Environmental Security Technology Certification Program (ESTCP). The publication of this report does not indicate endorsement by the Department of Defense, nor should the contents be construed as reflecting the official policy or position of the Department of Defense. Reference herein to any specific commercial product, process, or service by trade name, trademark, manufacturer, or otherwise, does not necessarily constitute or imply its endorsement, recommendation, or favoring by the Department of Defense.

Page Intentionally Left Blank

REPORT DOCUMENTATION PAGE

Form Approved
OMB No. 0704-0188

Public reporting burden for this collection of information is estimated to average 1 hour per response, including the time for reviewing instructions, searching existing data sources, gathering and maintaining the data needed, and completing and reviewing this collection of information. Send comments regarding this burden estimate or any other aspect of this collection of information, including suggestions for reducing this burden to Department of Defense, Washington Headquarters Services, Directorate for Information Operations and Reports (0704-0188), 1215 Jefferson Davis Highway, Suite 1204, Arlington, VA 22202-4302. Respondents should be aware that notwithstanding any other provision of law, no person shall be subject to any penalty for failing to comply with a collection of information if it does not display a currently valid OMB control number. **PLEASE DO NOT RETURN YOUR FORM TO THE ABOVE ADDRESS.**

1. REPORT DATE (DD-MM-YYYY) 06-15-2018		2. REPORT TYPE ESTCP Final Report		3. DATES COVERED (From - To) Oct. 2016 - Feb. 2018	
4. TITLE AND SUBTITLE Underwater Dynamic Classification Technology				5a. CONTRACT NUMBER W912HQ-16-C-0052	
				5b. GRANT NUMBER	
				5c. PROGRAM ELEMENT NUMBER	
6. AUTHOR(S) Jonathan S. Miller				5d. PROJECT NUMBER MR-201614	
				5e. TASK NUMBER	
				5f. WORK UNIT NUMBER	
7. PERFORMING ORGANIZATION NAME(S) AND ADDRESS(ES) White River Technologies, Inc. 115 Etna Rd., Building 3, Suite 1 Lebanon, NH 03766				8. PERFORMING ORGANIZATION REPORT NUMBER MR-201614	
9. SPONSORING / MONITORING AGENCY NAME(S) AND ADDRESS(ES) Environmental Security Technology Certification Program 4800 Mark Center Drive, Suite 17D08 Alexandria, VA 22350-3605				10. SPONSOR/MONITOR'S ACRONYM(S) ESTCP	
				11. SPONSOR/MONITOR'S REPORT NUMBER(S) MR-201614	
12. DISTRIBUTION / AVAILABILITY STATEMENT Distribution A: Approved for public release; distribution is unlimited.					
13. SUPPLEMENTARY NOTES					
14. ABSTRACT We performed this concept feasibility study to identify and examine the design features of an effective underwater dynamic classification EMI sensor. This examination included electromagnetic and hydrodynamic analyses to determine a sensor head configuration that will enable effective classification of UXO when operated in a hydrodynamically stable survey mode. Our analyses applied a combination of modeling and test-stand data collection to identify key design features and verify classification performance of an underwater towed system concept.					
15. SUBJECT TERMS Underwater Munitions Classification, Electromagnetic Induction					
16. SECURITY CLASSIFICATION OF:			17. LIMITATION OF ABSTRACT UU	18. NUMBER OF PAGES 83	19a. NAME OF RESPONSIBLE PERSON Jonathan S. Miller
a. REPORT UU	b. ABSTRACT UU	c. THIS PAGE UU			19b. TELEPHONE NUMBER (include area code) 603-678-8387

Page Intentionally Left Blank

FINAL REPORT

Project: MR-201614

TABLE OF CONTENTS

	Page
EXECUTIVE SUMMARY	ES-1
1.0 INTRODUCTION	1
1.1 BACKGROUND	1
1.2 OBJECTIVE OF THE STUDY	3
1.3 REGULATORY DRIVERS	4
2.0 TECHNOLOGY CONCEPT	5
2.1 CLASSIFICATION CONCEPT	6
2.2 DEPLOYMENT CONCEPT	8
2.3 ADVANTAGES AND LIMITATIONS OF THE TECHNOLOGY	9
3.0 PERFORMANCE OBJECTIVES	11
3.1 OBJECTIVE: MODEL ACCURACY	12
3.2 OBJECTIVE: EFFECTIVE EMI SENSOR CONFIGURATION	13
3.3 OBJECTIVE: EFFECTIVE UNDERWATER DYNAMIC CLASSIFICATION	13
3.4 OBJECTIVE: EFFECTIVE PROCESSING METHODS FOR THE UNDERWATER ENVIRONMENT	14
3.5 OBJECTIVE: ORIENTATION STABILITY	15
3.6 OBJECTIVE: POSITION STABILITY	15
3.7 OBJECTIVE: STANDOFF STABILITY	15
3.8 OBJECTIVE: DEPTH CONTROL RESPONSIVENESS	16
3.9 OBJECTIVE: OPERATING LOAD FEASIBILITY	16
3.10 OBJECTIVE: EFFECTIVE TARGET LOCATION TRACKING	17
4.0 TEST DESIGN	19
4.1 EMI TEST DESIGN	19
4.2 HYDRODYNAMIC TEST DESIGN	23
5.0 PERFORMANCE ASSESSMENT	29
5.1 OBJECTIVE: MODEL ACCURACY	29
5.2 OBJECTIVE: EFFECTIVE EMI SENSOR CONFIGURATION	33
5.3 OBJECTIVE: EFFECTIVE UNDERWATER DYNAMIC CLASSIFICATION	38
5.4 OBJECTIVE: EFFECTIVE PROCESSING METHODS FOR THE UNDERWATER ENVIRONMENT	40
5.4.1 Transmitter Loop Size	41
5.4.2 Standoff	42
5.4.3 Depth	43
5.4.4 Sea Surface	44

TABLE OF CONTENTS (Continued)

	Page
5.4.5 Conclusion	45
5.5 OBJECTIVE: ORIENTATION STABILITY	46
5.5.1 Roll Response	46
5.5.2 Pitch Response	47
5.5.3 Conclusion	47
5.6 OBJECTIVE: POSITION STABILITY	48
5.6.1 Sway Response	51
5.6.2 Heave Response	52
5.6.3 Conclusion	53
5.7 OBJECTIVE: STANDOFF STABILITY	53
5.8 OBJECTIVE: DEPTH CONTROL RESPONSIVENESS	55
5.9 OBJECTIVE: OPERATING LOAD FEASIBILITY	56
5.10 EFFECTIVE TARGET LOCATION TRACKING.....	57
6.0 COST ASSESSMENT.....	59
7.0 CONSIDERATIONS FOR IMPLEMENTATION	61
7.1 CONSIDERATIONS FOR UNDERWATER DYNAMIC CLASSIFICATION.....	61
7.2 CONSIDERATIONS FOR TOWED OPERATION	62
7.3 CONCLUSION.....	62
8.0 REFERENCES	63
APPENDIX A UNDERWATER TOWED ARRAY DRAWINGS	A-1

LIST OF FIGURES

	Page
Figure 1. A Dynamic Classification Survey Using the OPTEMA Towed Sensor at the Former SWPG (left) Produced a 95% Clutter Rejection Rate at Maximum Operating Efficiency (100% UXO Correctly Classified) as Shown in the ROC Curve (right)...	2
Figure 2. The OPTEMA Sensor Head Creates Optimal Classification Regions Across the Entire Array Swath.....	2
Figure 3. The Marine Magnetics Seaquest is an Example of an Effective Underwater 3D Form Factor (www.marinemagnetics.com).	3
Figure 4. Towed Classification Array Concept.	5
Figure 5. A Comparison of Dynamic Classification Methods.....	7
Figure 6. Using the Single Shot Dynamic Approach, Each Anomaly (SWPG2-40 Shown Here) Is Assigned a Cluster Comprising the Polarizabilities (left) and Estimated Source Locations (right).	7
Figure 7. Example of a Variable Line Towed Sensor.....	8
Figure 8. Magnetometer Data Acquired During a DGM Survey.	9
Figure 9. Example of Real and Synthetic Data Noise Characteristics.....	20
Figure 10. X-coil Design.	21
Figure 11. Y-coil Design.	21
Figure 12. Z-coil Design.	22
Figure 13. Receiver Locations.	22
Figure 14. Typical Noise Standard Deviation Measured in Dynamic OPTEMA Survey Data..	23
Figure 15. Proposed Bridle Configuration.....	24
Figure 16. Towing System Global Frame and Body-fixed Coordinate Frame.....	25
Figure 17. Free Body Diagram Illustrating the Forces Acting on the Tow Body System.....	25
Figure 18. A 2/3-scale Mockup of the Underwater Towed Array Concept.	29
Figure 19. Noise Standard Deviation Values Corresponding to 90 Receiver Channels as a Function of Time Gate (Horizontal Axis).	30
Figure 20. Grid-based Test Stand Data Collection.	30
Figure 21. LEFT: Library Match Metric Applied to OPTEMA SWPG Data from a 20mm Projectile Encounter. RIGHT: Library Match Metric Applied to Approximately 2000 Anomaly Encounters at Southwestern Proving Ground.....	31
Figure 22. Library Match Metric for 30 Grid Locations.	32
Figure 23. Example of Well Constrained Polarizabilities.	32
Figure 24. Example of Poorly Constrained Polarizabilities.	33
Figure 25. Diagram of Modifications Made to OPTEMA Design for the Underwater Towed Configuration.....	33
Figure 26. Transmitter Field Principal Component Distributions 15 cm Below the Sensor.	34
Figure 27. Transmitter Field Principal Component Distributions 1.0 m Below the Sensor.	35
Figure 28. Diagram of Simulation Design.....	36
Figure 29. LEFT: Synthetic Dynamic Data Corresponding to 105-mm Projectile Encounter at 1-meter Depth.	36

LIST OF FIGURES

	Page
Figure 30. LEFT: Synthetic Dynamic Data Corresponding to 105-mm Projectile Encounter at 1.8-meter Depth. RIGHT: Polarizability Cluster from Synthetic Data Soundings Compared to 105-mm Library.....	37
Figure 31. Library Match Results from 250+ Simulations of Dynamic Encounters with Three TOI.	37
Figure 32. LEFT: Simulated Dynamic Towed Overpass for a 155-mm TOI Encounter. TOP RIGHT: Inversion Results for the Dynamic Test Stand Data with 10cm Position Error added. BOTTOM RIGHT: Inversion Results for the Dynamic Test Stand Data with 75cm Position Error Added.	39
Figure 33. Library Match as a Function of Added Position Error.	40
Figure 34. This Figure Describes the Basic Model Parameters.....	41
Figure 35. Sphere Response for Various Loop Sizes.	42
Figure 36. Sphere Response for Various Standoff Heights.	43
Figure 37. Sphere Response for Various Depths of the Sphere Below Seafloor.....	44
Figure 38. In-phase (I) and Quadrature-phase (Q) Response at 1 kHz and 10 kHz Corresponding to the Seafloor and Sea Surface Interaction with the Transmitter Field at Various Sensor Depths.	45
Figure 39. Load Case S-01, Roll Response of the Towed EMI Sensor.....	46
Figure 40. Load Case S-02, Pitch Response of the Towed EMI Sensor.	47
Figure 41. Setup of Towed Sensor Array in Virtual Wind Tunnel, with Refinement Zones Shown.	48
Figure 42. Streamlines of Towed Sensor Generated in Virtual Wind Tunnel.....	49
Figure 43. Velocity Magnitude Demonstrating the Shielding Effect Captured in Virtual Wind Tunnel.....	49
Figure 44. Drag Force as a Function of Flow Speed for the Towed Array Sensor with a Pitch Angle of 0 Degrees.....	50
Figure 45. Load Case S-03, Sway Response of the Towed EMI Sensor with 1.5 m/s Tow Speed.	52
Figure 46. Load Case S-04 (Blue) and S-05 (Green), Heave Response of the Towed EMI Sensor (Rising and Falling) with 1.5 m/s Tow Speed.....	53
Figure 47. Load Case S-06 and S-07, Heave Position of the Towed EMI Sensor in Waves (Head and Following) with a 1.5m/s Tow Speed.....	54
Figure 48. Load Case S-06 and S-07 Tow Point Heave Position.	54
Figure 49. Layback Error as a Function of Depth Measurement Error at 30-meter Operating Depth.	57

LIST OF TABLES

	Page
Table 1.	EMI-based Classification Performance Objectives. 11
Table 2.	Hydrodynamic Performance Objectives. 12
Table 3.	Towed EMI Sensor Mass Properties..... 26
Table 4.	Component Principal Dimensions and Total Volume. 26
Table 5.	Simulated Load Cases for the Hydrodynamic Performance Assessment..... 27
Table 6.	Case 1: Transmitter Loop Parameters..... 41
Table 7.	Case 2: Standoff Parameters 43
Table 8.	Case 3: Depth Parameters 44
Table 9.	Drag Area Results from VWT, drag Coefficients Required in ProteusDS..... 50
Table 10.	Towline Tensions for Load Case S-06 and S-07. 55
Table 11.	Tow Speed, Clump Weight, and Vertical Velocity of Control Load Cases. 55
Table 12.	Layback and Towline Tensions for Load Cases O-01 to O-04. 56
Table 13.	Towline Tensions During Start Case O-07..... 56
Table 14.	Mean Location Error and Standard Deviation for TOI Location Estimates..... 58

Page Intentionally Left Blank

ACRONYMS AND ABBREVIATIONS

ADC	Analog to Digital Converter
APG	Aberdeen Proving Ground
CB	Center of Buoyancy
CFD	Computational Fluid Dynamics
CG	Center of Gravity
DGM	Digital Geophysical Mapping
DOF	Degree of Freedom
DSA	Dynamic Systems Analysis
EMI	Electromagnetic Induction
GPS	Global Positioning System
IMU	Inertial Measurement Unit
MBUD	Marine Berkeley UXO Discriminator
OPTEMA	One Pass Time domain EMI Array
RTK	Real Time Kinematic
SNR	Signal to Noise Ratio
SWPG	Southwestern Proving Ground
TOI	Target of Interest
UXO	Unexploded Ordnance
VWT	Virtual Wind Tunnel
WRT	White River Technologies

ACKNOWLEDGMENTS

This project benefitted from the valuable input from our collaborators at Dynamic Systems Analysis Ltd. (DSA) and the Woods Hole Oceanographic Institute (WHOI). Andrew Baron and Dean Steinke, both from DSA, provided the hydrodynamic modeling and simulation expertise to support the operational analyses of the towed sensor concept. Hendrik Muller (WHOI) performed extensive numerical and analytical modeling to evaluate the feasibility of applying electromagnetic induction processing methods to the underwater environment.

EXECUTIVE SUMMARY

We performed this concept feasibility study to identify and examine the design features of an effective underwater dynamic classification EMI sensor. This examination included electromagnetic and hydrodynamic analyses to determine a sensor head configuration that will enable effective classification of UXO when operated in a hydrodynamically stable survey mode. Our analyses applied a combination of modeling and test-stand data collection to identify key design features and verify classification performance of an underwater towed system concept.

This concept feasibility study culminated with the design of an underwater dynamic classification sensor based on advanced EMI principles. This design has been optimized specifically for meeting the increased standoff requirements for underwater towed operation. Our electromagnetic analysis results demonstrated that the dynamic classification methods used on land are applicable to underwater operations and can achieve high quality classification at the increased standoff range. Significant findings of our electromagnetic analysis include:

1. Reliable classification (i.e., constraint of all principal polarizabilities) can be achieved for all across track offsets within the sensor swath of 3 meters.
2. It will be necessary to increase the effective transmitter power from 100 A-turns to at least 200 A-turns to accommodate increased standoff operation.
3. Predicted standoff range to target for which reliable classification can be achieved at the 200 A-turn power level: 81mm – 1.4m; 105mm – 1.8m; 155mm – 2.4m.
4. Dynamic classification processing methods, including background correction, used on land will be applicable in the underwater environment. The exception may be background correction at the earliest time gates (<200-500 microseconds), where seawater and target interaction may preclude conventional background subtraction. We do not believe this portion of the time decay will be important for classification since our system measures the decay out to 8.3ms.

Our hydrodynamic analysis results demonstrated that the 3D transmitter configuration provides a hydrodynamically stable design due to the increased metacentric height. Drag forces will not be significant or prohibitive for towed operation at the targeted survey speed (2-4 knots). Significant findings of our hydrodynamic analysis include:

1. Tow point heave due to surface conditions should have a minimal impact on seafloor standoff variability (+/- 15cm in worst case operating conditions); however, our simulations indicated that heave may cause a net offset in standoff. This offset can be compensated for with towline length adjustment.
2. Depth control responsiveness varies considerably with towline angle. Higher tow speeds (more drag) produce more layback and a lower towline angle, which reduces the vertical component of the winch pay-in velocity. Our simulations indicate that responsiveness to seafloor inclines of 10 degrees should be obtainable under typical survey conditions. For greater responsiveness to seafloor variability, lower speeds or larger clump weights should be applied.

3. Sensor position error will most likely be the greatest contributor to overall (global) target localization error. Accurate measurement of the sensor depth will be critical. Additionally, if cable catenary is significant, towline tension will need to be monitored to adjust for these line length offsets. Our analysis indicates that cumulative target localization error (i.e., combined error from inversion and sensor position tracking) can be limited to 0.5m or better.

1.0 INTRODUCTION

This project was undertaken by White River Technologies, Inc. (WRT) to address the critical need for advancements in technologies that will enable detailed underwater surveys to the extent that classification may be implemented effectively. While classification methods have demonstrated tremendous success in reducing false alarm rates and unnecessary excavations following terrestrial electromagnetic induction (EMI) surveys, these performance gains have yet to be fully realized in underwater environments. Several factors contribute to this capability gap including the need to adapt land-based classification models to the underwater environment; however, it can be argued that the greatest obstacle to achieving underwater classification success at this time is the complexity and cost associated with deployment of classification-level EMI sensors in this environment.

Traditionally, classification-level (i.e., advanced) EMI sensors have been successfully deployed using the two-step detection/cued approach during land-based surveys. For such surveys, the cued method works because it is a relatively efficient process to reacquire each anomaly location with an advanced sensor on land; however, placing advanced sensors over underwater targets is significantly more difficult. During underwater surveys, non-GPS positioning constraints are compounded by the challenges associated with the actual sensor deployment. Even if accurate position information is achieved with non-GPS techniques (e.g., acoustic methods), placement of the sensor in close proximity to the target pick location requires complicated and/or costly survey methods. Remotely operated vehicles (ROVs), divers, and surface vessels with winch systems are all possibilities for deploying cued sensors underwater; however, none of these methods offers the ease-of-use that is enabled by the land-based cued survey platforms.

The challenges of implementing advanced EMI surveys underwater were highlighted in a recently released SERDP Final Project Report MR-2321. During the Phase II demonstration of the Marine Berkeley Unexploded Ordnance Discriminator (MBUD), system demonstrators determined that using the surface vessel to position the sensor in the predetermined seed location would be difficult to achieve (given the project scope) and instead relied on diver supported positioning of the sensor in subsequent underwater demonstrations (Morrison, 2014). In addition to these positioning and deployment challenges, underwater cued surveys may also present a significant workflow limitation: in some cases, hydrodynamic forcing and associated munitions mobility may significantly alter the positioning requirements developed during the initial mapping survey. In other words, if there are significant delays between the digital geophysical mapping (DGM) and cued surveys, it is possible that some targets may shift from their “cued” locations making a follow-up cued survey of these items ineffective. These aforementioned survey challenges and limitations warrant a consideration of efficient and cost-effective underwater survey methodologies, such as dynamic classification, that would minimize total survey time.

1.1 BACKGROUND

The basis for an underwater dynamic classification sensor concept is an approach that we applied to munitions response surveys on land. Under project MR-201225, we demonstrated and validated a one-pass survey method using the OPTEMA advanced EMI sensor. Through technology and live site demonstrations performed at Aberdeen Proving Ground (APG) and the former Southwestern Proving Ground (SWPG), we demonstrated that one-pass, dynamic classification could provide results comparable to those achieved during cued EMI sensor surveys in a fraction of the survey time (Hill et al., 2014), (Miller, 2017).

For example, at the SWPG live site demonstration, we surveyed a 4-acre area containing several thousand anomalies over a period of two days. We then inverted the dynamic data for polarizabilities that allowed us to classify each anomaly and make a dig/no-dig decision. This approach yielded an 82% clutter rejection rate (at the stop dig point) with 100% correct identification of UXO items on a sample size of approximately 2000 anomalies (Figure 1).

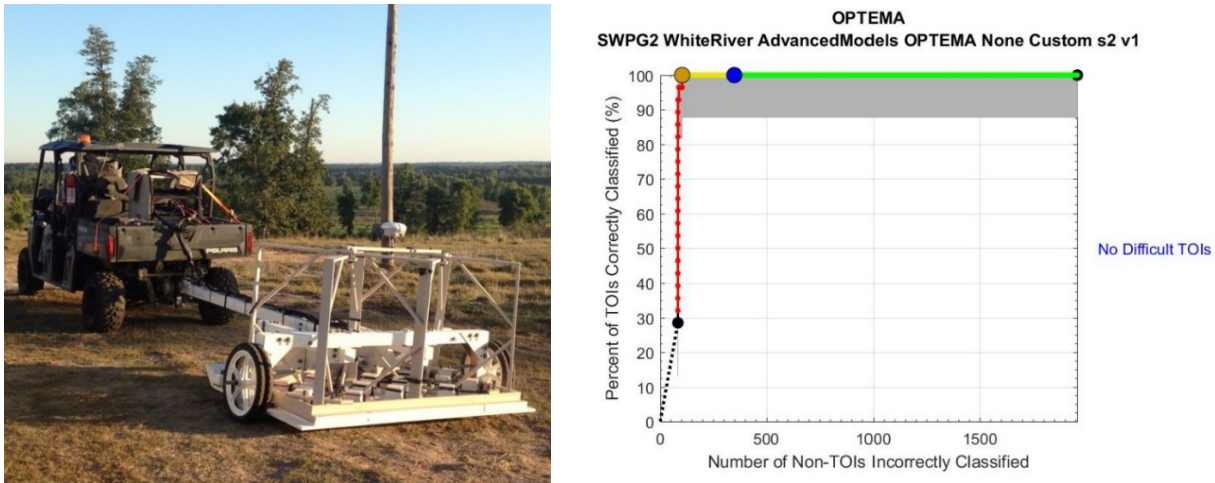


Figure 1. A Dynamic Classification Survey Using the OPTEMA Towed Sensor at the Former SWPG (left) Produced a 95% Clutter Rejection Rate at Maximum Operating Efficiency (100% UXO Correctly Classified) as Shown in the ROC Curve (right).

These results are comparable to those achieved using cued survey practices.

A key factor in achieving these results was a sensor design that enabled effective dynamic classification. The OPTEMA sensor head comprises five transmitters and fourteen 3-axis receivers across a 1.8-meter sensor swath. This design ensures that three orthogonal magnetic fields are produced at any across track location, a critical requirement for dynamic classification (Figure 2). The distribution of the 14 receivers also ensures that fields scattered by any target located across the sensor swath will be characterized sufficiently to constrain inversion of the data.

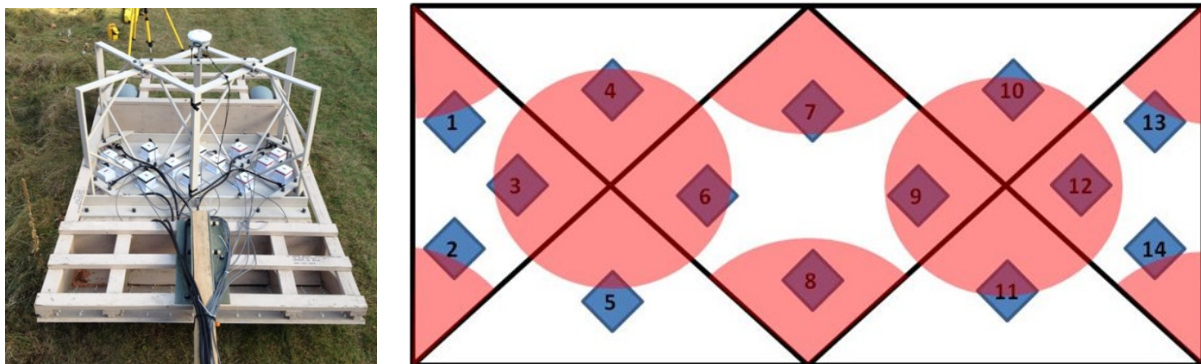


Figure 2. The OPTEMA Sensor Head Creates Optimal Classification Regions Across the Entire Array Swath.

Classification is performed on soundings acquired while the sensor array was positioned such that the target was located beneath one of the highlighted regions. These regions correspond to areas of greater orthogonality between transmitter fields.

Applying a similar classification approach may be ideal for underwater surveys since this approach does not require follow-up cued surveys after the mapping stage; however, to achieve these results underwater, a towed sensor design that is hydrodynamically feasible must be implemented. While the OPTEMA is well-suited for land surveys, its form factor may not be optimal for underwater towed surveys. There is certainly precedent for underwater 3D towed sensors (e.g., Figure 3); however, these designs require consideration of hydrodynamic lift and drag forces for proper implementation. Accordingly, design of an effective underwater dynamic classification sensor will require a detailed and careful analysis of both the electromagnetic and hydrodynamic features that will influence overall performance.

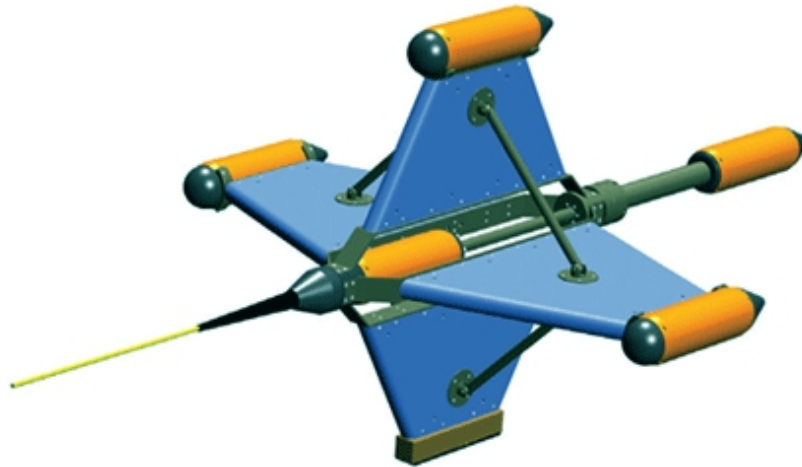


Figure 3. The Marine Magnetics Seaquest is an Example of an Effective Underwater 3D Form Factor (www.marinemagnetics.com).

1.2 OBJECTIVE OF THE STUDY

The primary objective of this study was to identify and examine the design features of an effective underwater dynamic classification EMI sensor. This examination included electromagnetic and hydrodynamic analyses to determine a sensor head configuration that will enable effective classification of UXO when operated in a hydrodynamically stable survey mode. Our analyses applied a combination of modeling and laboratory/test-stand data collection to identify key design features and verify classification performance of an underwater towed system concept.

It should be noted that this design study leverages the work of previous and ongoing SERDP/ESTCP-funded underwater phenomenology studies (e.g., MR-2728, PI: Shubitidze; MR-2409, PI: Bell; MR-2412, PI: Billings; and MR-1714, PI: Schultz) and is, therefore, not intended as a comprehensive phenomenology assessment. Instead, our specific objectives focused on evaluating the requirements for adapting land-based dynamic classification methods to the underwater environment, assessing the hydrodynamic factors critical to a towed array configuration, and developing the design features that fully exploit the information gleaned from these analyses. We did include some analysis of seawater/field interactions, but in the context of applying land-based classification methods, namely background removal techniques, to the dynamic underwater environment.

1.3 REGULATORY DRIVERS

The main benefit to the DoD would be to facilitate the cleanup of underwater munitions contamination areas by significantly reducing the cost of these remediation operations. The cost reductions enabled by classification technologies have been well documented and demonstrated on land. It can be argued that these cost savings would be even greater for underwater sites as reacquisitions and intrusive investigations are much more difficult to implement underwater. Any technologies that streamline operations associated with underwater munitions classification could have a large impact on the DoD's ability to effectively implement these technologies.

2.0 TECHNOLOGY CONCEPT

Our concept is to employ an advanced EMI design that will enable dynamic classification from a hydrodynamically stable towed configuration. This concept requires two significant adaptations to the land-based dynamic system:

1. A modified form factor. Aside from the hydrodynamic factors that influence sensor form, the underwater environment also presents operational factors that require modifications to land-based designs. For example, due to the large areas and lack of vegetation, a wider swath (i.e., larger transect spacing) is typically desired for underwater survey systems.
2. A modified sensing range. While land-based sensors can be placed at ground level, underwater towed sensors must operate above the seafloor, typically at a minimum standoff of 0.5-1.0 meters or more. Therefore, the sensor range must be modified to detect and classify at ranges that may exceed those required on land.

Figure 4 shows a drawing of our underwater sensor concept. The basic components include 7 transmitters (4 in the X -direction, 2 in the Y -direction, and 1 Z -directed), 15 (3-axis) receivers, and transmit and data acquisition electronics. The design features 4-point two bridle configurations as well as lifting surfaces along the leading and trailing edges of the array to assist roll and sway stabilization. The concept also includes a pair of electronics bottles that house transmit and ADC electronics located on top of the sensor to elevate the center of buoyancy, which also increases stability.

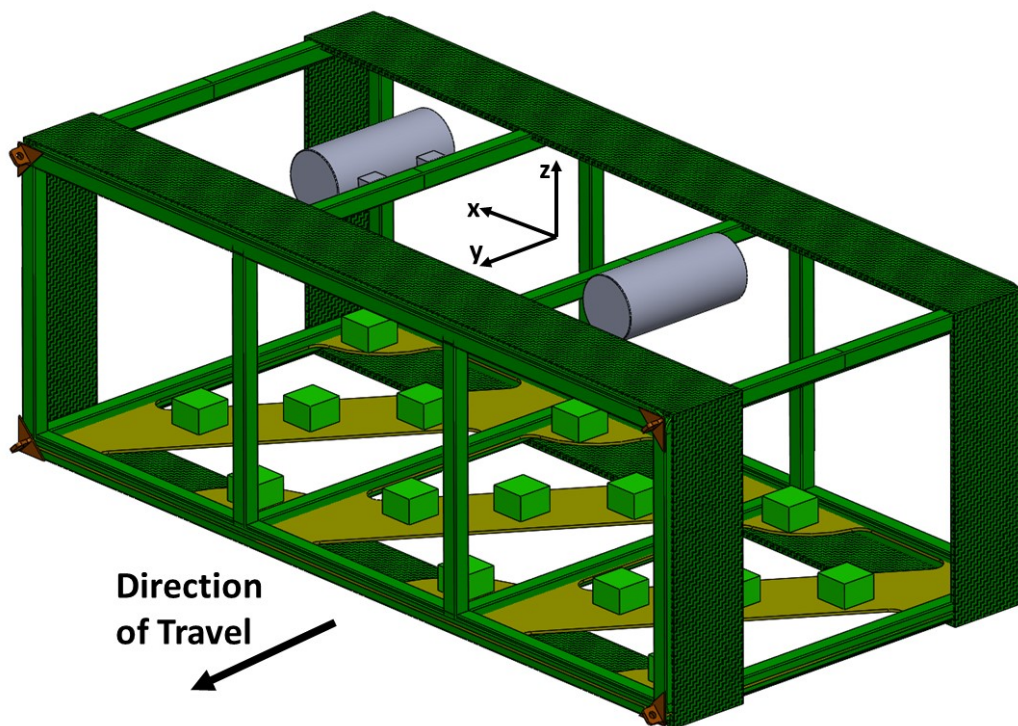


Figure 4. Towed Classification Array Concept.

The array covers a 3-meter swath with 7 transmitters and 15 (3-axis) receivers. Electronics bottles are mounted on top to raise the center of buoyancy.

Overall dimensions of the array are 3.0m x 1.5m x 1.0m (Width x Length x Height or $X \times Y \times Z$). The array frame comprises 2.5-inch square tubing, which will serve two purposes: 1) to act as rigid structural members; and 2) to provide insulated formers for the transmitter wire. Previous underwater phenomenology studies have demonstrated that insufficient transmitter wire insulation against seawater can increase the coil capacitance enough to reduce current damping after shutoff and increase noise levels (e.g., Bell et al., 2016; Billings et al., 2016). We have selected frame members that will be appropriately sized to provide structural support and electrical insulation against seawater. Detailed drawings of the frame design are provided in the Appendix.

2.1 CLASSIFICATION CONCEPT

As discussed in Section 1.1, we base our underwater dynamic classification concept on the dynamic classification principles validated during the MR-201225 live site demonstration. This approach is well suited for the underwater environment for two significant reasons:

1. All classification features for an anomaly can be extracted from one pass over the target, obviating the need for a cued reacquisition, which may present the aforementioned challenges in an underwater environment; and
2. Classification features can be obtained without the need for precise positioning information (e.g., RTK-quality GPS), which may be challenging to acquire underwater.

The latter consideration results from a key aspect of our concept design, namely, that the sensor array provides effective multi-axis illumination (i.e., orthogonal transmitter field components) of an object that is positioned at any location beneath or in proximity to the array. This “single-shot” approach relies only on the coordinate frame of the sensor head to ensure that accurate classification features can be extracted from any sounding acquired over the object (Figure 5). This method differs from the “multi-shot” approach, which aggregates data from multiple soundings to obtain the required multi-axis illumination. While the multi-shot approach can provide high quality classification features, it relies on multiple positions of the sensor head, which must be accurately tracked with respect to an arbitrary fixed reference frame and, therefore, requires a high degree of relative positioning accuracy between successive measurements. This requirement may pose a challenge underwater.

The single shot dynamic approach produces a unique set of electromagnetic polarizabilities (classification features) corresponding to each measurement location. In addition to these polarizabilities, the data inversion also produces a source location (vector r_{0m} in Figure 5) corresponding to each measurement location. Classification of the target can be performed by clustering similar source locations and polarizability sets in a group assigned to the anomaly. In this sense, a “cluster” refers to multiple similar polarizability sets associated with one anomaly. We have developed a classification ranking method that uses these clusters to assign a target of interest (TOI) confidence value by selecting the best polarizability match to a TOI library from the cluster group. Figure 6 shows an example of the cluster-based classification from SWPG data.

This classification approach could offer a robust solution for underwater surveys where the positioning accuracy required for multi-shot classification or cued deployment may be difficult to achieve. Additionally, the ability to resolve classification features from a single, dynamic pass over the target could be beneficial for environments where costs or operations associated with cued reacquisition may be prohibitive.

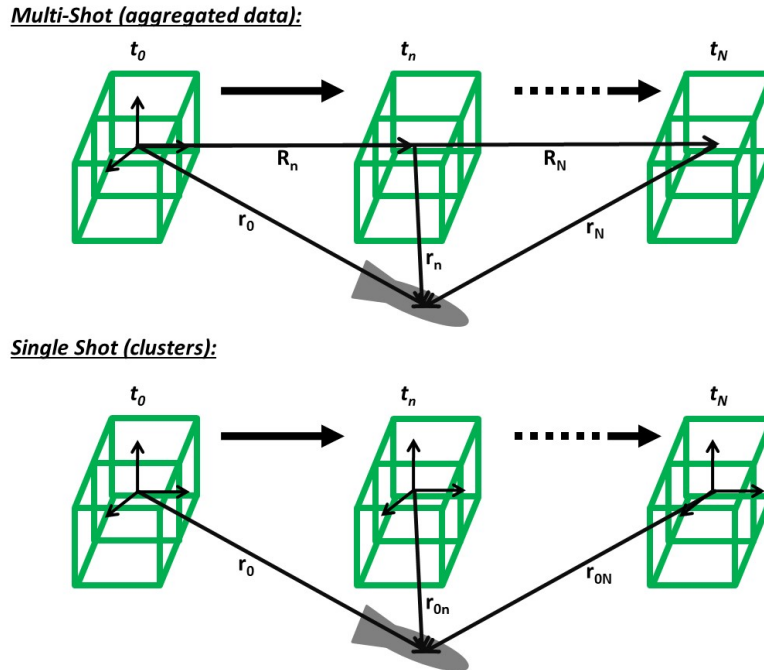


Figure 5. A Comparison of Dynamic Classification Methods.

In both the multi-shot and single shot approaches, the vector r_n or r_{0n} is extracted from the inversion of data. In the multi-shot approach, however, the data used for inversion are aggregated from multiple measurement locations and, therefore, a relative position vector R_n must be accurately measured with respect to a starting reference frame as well. In the single shot approach, each measurement location provides a complete data set for inversion and produces a unique set of classification features that can be clustered with features from the other measurement locations. No relative position measurements are needed using this classification approach.

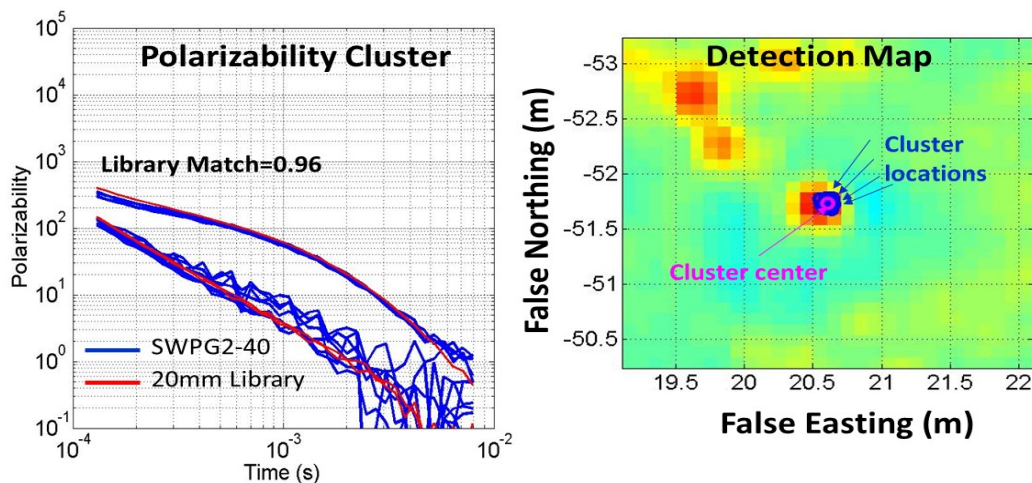


Figure 6. Using the Single Shot Dynamic Approach, Each Anomaly (SWPG2-40 Shown Here) Is Assigned a Cluster Comprising the Polarizabilities (left) and Estimated Source Locations (right).

A TOI confidence value is based on the library match metric, which identifies the closest match to a TOI library from each cluster.

2.2 DEPLOYMENT CONCEPT

Dynamic classification surveys, from an operational perspective, are similar to the wide area or Digital Geophysical Mapping (DGM) surveys that have been successfully implemented in underwater environments from various tow-vessels or underwater vehicles (Schultz et al., 2011; Steigerwalt et al., 2014; Funk et al., 2011; McDonald, 2008). While these surveys do not typically afford the centimeter level positioning accuracy required for cued deployment, they do regularly achieve the sub-meter accuracy necessary for anomaly detection and diver/ROV reacquisition. Our deployment concept, therefore, focuses on implementing the aforementioned single shot, dynamic approach from DGM surveys performed in the underwater environment.

The concept for deployment of the sensor head shown in Figure 4 employs a passive tow body design with variable line length to set the sensor depth. Depending on the tow speed and desired depth, the tow line length can be adjusted so that the line angle produces the required forces to maintain equilibrium at the desired depth (Figure 7).

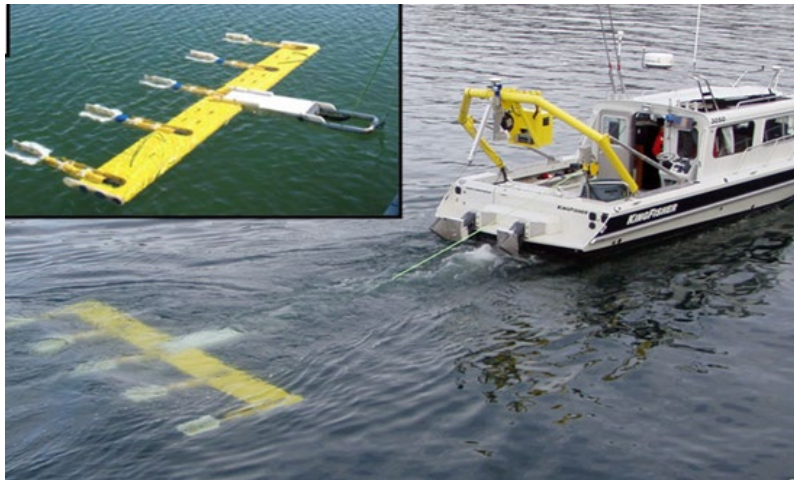


Figure 7. Example of a Variable Line Towed Sensor.

This magnetometer array is part of a passive tow wing that uses winch cable pay-out to adjust sensor depth (from Schultz et al., 2011).

A sensor head altimeter provides continuous feedback regarding sensor height above the seafloor. To raise or lower the sensor at a given, fixed survey speed, the winch line is shortened or lengthened. Positioning can be accomplished through kinematic transformation of the tow body altitude, tow azimuth angle, and line length measurements to global coordinates using the surface vessel GPS and winch encoder outputs. This method has been successfully applied with previous underwater magnetic surveys to achieve 15-20 cm global accuracy and maintain depth within +/- 10 cm of the desired value (see Schultz et al., 2011 and supporting data in Figure 8).

We believe the positioning accuracy afforded by this approach will be sufficient for detection and diver reacquisition for recovery. Therefore, combining the single shot, dynamic classification approach with this deployment method should enable effective recovery of potential TOI. Because the positioning accuracy is not critical for classification performance (using the single shot approach), it need only be sufficient to direct reacquisition of UXO.

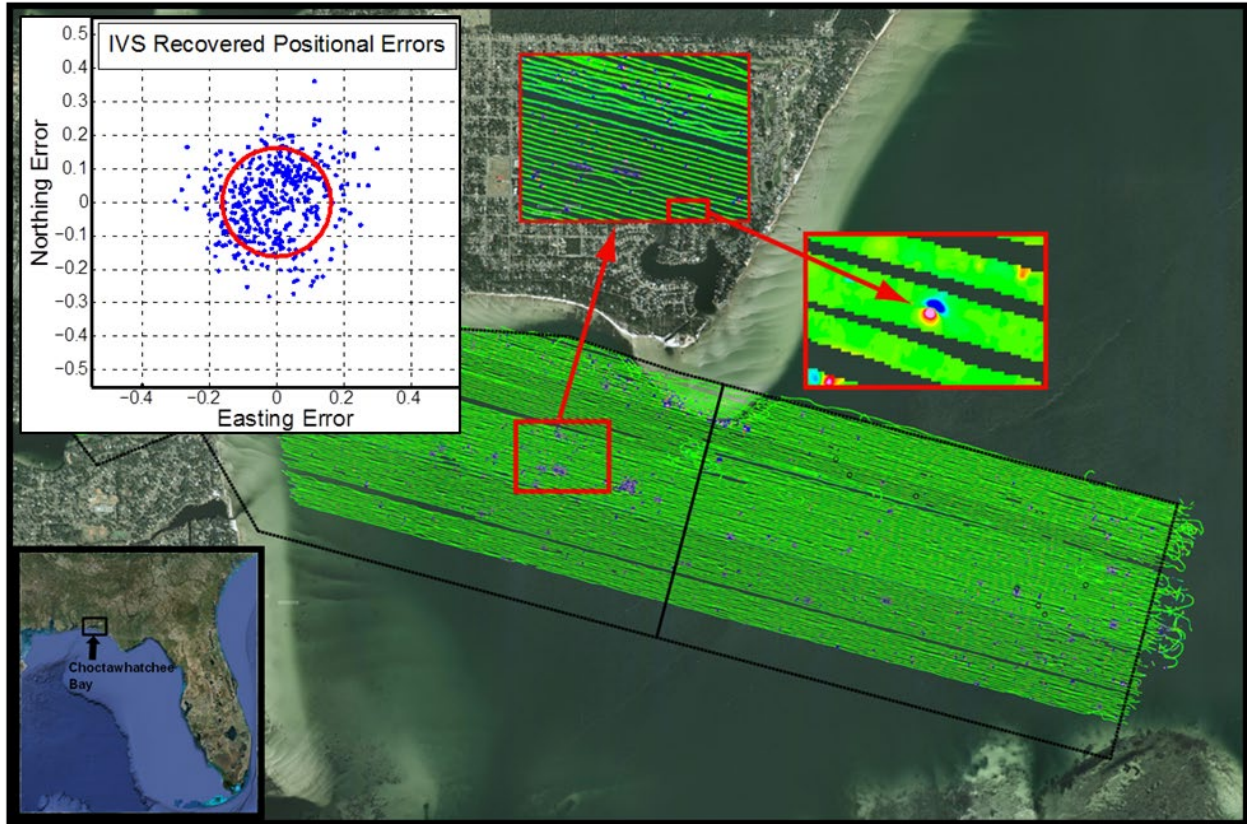


Figure 8. Magnetometer Data Acquired During a DGM Survey.

Georegistration of the data applies kinematic transformation of the sensor array with respect to the GPS on the surface vessel. This method has been shown to enable better than 0.5m accuracy for recovering position of anomalies (from Schultz et al., 2011).

2.3 ADVANTAGES AND LIMITATIONS OF THE TECHNOLOGY

The primary advantage of the dynamic classification technology over the cued EMI approach is the ability to acquire effective classification data in one-pass dynamic mode. This capability means that the towed system could deliver detection and classification in what would effectively be a DGM survey mode, thus eliminating the need for a secondary cued survey. The removal of this cued step could be particularly cost effective for underwater surveys where cued reacquisitions could be difficult to implement due to underwater positioning constraints and costly due to diver or ROV reacquisition costs.

The main limitation of the approach is the potential reduction in signal-to-noise ratio (SNR). Compared to cued surveys, dynamic sensors spend less time over the target and, therefore, accumulate fewer samples for stacking and noise reduction. Additionally, in the case of underwater surveys, a dynamic towed sensor may require significantly more standoff from the target when compared to a cued sensor that could be placed directly on the seafloor. We believe these potential disadvantages related to inherently lower SNR can be overcome through optimal design of sensor features, such as coil size and transmitting power, as well as through data processing strategies, such as filtering.

Page Intentionally Left Blank

3.0 PERFORMANCE OBJECTIVES

For this design study, we assessed the potential performance of an underwater dynamic classification sensor using several quantitative performance metrics. We set specific objectives related to both the hydrodynamic performance and the electromagnetic capabilities of the system. We assessed performance through modeling, simulation, and basic experimentation. Table 1 and Table 2 list the performance objectives for this study.

Table 1. EMI-based Classification Performance Objectives.

Performance Objective	Metric	Data Required	Success Criteria
EMI-Based Classification Performance Objectives			
Model Accuracy	Model prediction of classification performance	<ul style="list-style-type: none"> Model predictions and test stand data corresponding to relevant 3D EMI sensor configuration 	Model-based library match predictions consistent with library matches recovered from test stand data
Effective EMI Sensor Configuration	Library match metric	<ul style="list-style-type: none"> Synthetic data corresponding to towed sensor configuration encounters with targets at standoffs >1 meter 	Library match >0.9 for polarizabilities corresponding to TOI >1 meter from sensor bottom
Effective Underwater Dynamic Classification	Library match metric	<ul style="list-style-type: none"> Test stand data with positional error added to simulate underwater positioning constraints 	Library match >0.9 for polarizabilities corresponding to data with added positional errors
Effective Processing Methods for the Underwater Environment	Background response	<ul style="list-style-type: none"> Simulation of seawater, sensor, and target interactions 	Demonstration of effective background removal technique for underwater environment

Table 2. Hydrodynamic Performance Objectives.

Performance Objective	Metric	Data Required	Success Criteria
Hydrodynamic Performance Objectives			
Orientation stability	Roll and pitch righting response to perturbation	<ul style="list-style-type: none"> Simulation of pitch and roll angles after initial offset condition 	Settles to within +/- 5 degree pitch and roll after initial perturbation
Position stability	Heave and sway transient response to perturbation	<ul style="list-style-type: none"> Simulation of heave and sway offset after initial offset condition 	Settles to within 0.5m (lateral) and 0.15m (vertical) of neutral position after initial perturbation
Standoff stability	Heave offset during worst-case operating conditions	<ul style="list-style-type: none"> Simulation of heave motion in Sea State 3 	Maintains seafloor standoff within +/-15 cm variability
Depth control responsiveness	Vertical velocity as a function of winch pay-in	<ul style="list-style-type: none"> Simulation of vertical velocity in response to winch pay-in 	Responsive to seafloor slope of up to 10% incline
Operating load feasibility	Towline tension	<ul style="list-style-type: none"> Simulation of towline tension under typical start, stop, and steady state conditions 	Ensure operating loads are within specification limits for standard towline and winch components
Effective target location tracking	Target localization error	<ul style="list-style-type: none"> Estimates of cumulative sensor and target location error 	Overall target location error <0.5 meter

3.1 OBJECTIVE: MODEL ACCURACY

A performance assessment that is based on synthetic data or simulations requires verification of the model accuracy. Because much of our classification performance assessment is based on models of a full-scale sensor configuration, we wanted to first verify that our model predictions agreed with actual sensor data.

Data Requirements

We fabricated a 2/3-scale sensor array and collected test stand data to which we applied classification processing. We then compared these classification results to predictions from our sensor model. The model included the basic features of the sensor design (e.g., transmitter size, receiver location, etc.) as well as noise estimates acquired from actual sensor data.

Metric

This objective applies a classification performance metric. Classification performance is quantified by comparing polarizabilities obtained from real or synthetic data to the corresponding TOI library polarizabilities (i.e., using a library match metric). The classification performance metric is a measure of the consistency between the predicted library match and the observed library match.

Success Criteria

Because we want to accurately predict when the data will result in a well constrained or a poorly constrained inversion, we want to ensure that the model can distinguish high quality classification (well constrained) from low quality classification (poorly constrained). While many factors can influence the library match value (for example, did we use the appropriate library for the data?), in this study, the library match metric is a good indicator of the sensor's overall classification performance. We match the polarizabilities from a known TOI to the appropriate library and the quality of our data (both synthetic and real) is primarily influenced by the sensor configuration and the sensor noise levels. Therefore, a high match value (e.g., 0.9 or higher) would indicate that the sensor provides a configuration that enables good classification performance while a low match value (e.g., <0.8) would indicate that the sensor provides a configuration that leads to unreliable classification. The library match metric can produce a value between 0 (very poor match) to 1 (perfect match). We consider the model successful if it provides a match value that is within 5% of the observed match value for values >0.8.

3.2 OBJECTIVE: EFFECTIVE EMI SENSOR CONFIGURATION

One of our key objectives for this study is to identify an EMI sensor configuration that will enable reliable classification from a dynamic survey mode. Given the constraints of operating in an underwater environment, we anticipate that it will be necessary to maintain a seafloor standoff of at least 1 meter. Therefore, we want to assess classification performance for target encounters occurring at or exceeding this range.

Data Requirements

After we have confirmed the model accuracy, we will use the model to create synthetic data from a full-scale underwater array encountering TOI (sized 81-mm and larger) at standoffs of 1 meter or more. We will then apply our dynamic classification processing flow to these data to recover polarizability clusters that can be compared to the appropriate TOI library to determine a match metric value.

Metric

This objective applies the library match metric.

Success Criteria

A match metric value of 0.9 or higher will indicate effective classification.

3.3 OBJECTIVE: EFFECTIVE UNDERWATER DYNAMIC CLASSIFICATION

As discussed earlier, an additional challenge for operating in the underwater environment is the lack of high-quality GPS positioning that is used to track sensor head location during land surveys. Instead, we will rely on kinematic transformation with respect to a GPS on the surface vessel. While this method should provide sufficient positioning accuracy to detect and reacquire anomalies, we do not expect that it will provide the <2cm accuracy enabled by differential, RTK GPS tracking. Therefore, to assess the effects of this somewhat degraded positioning quality, we will introduce position errors to the data. We will then invert the modified data and assess the quality of the resulting polarizabilities.

Data Requirements

We will collect dynamic test stand data with known positions of the TOI. We will add errors to these data and invert using our standard dynamic classification processing flow.

Metric

This objective applies the library match metric.

Success Criteria

A match metric value of 0.9 or higher for position errors (between consecutive samples) of up to 15 cm will indicate effective classification.

3.4 OBJECTIVE: EFFECTIVE PROCESSING METHODS FOR THE UNDERWATER ENVIRONMENT

A key assumption in the implementation of the dynamic classification processing flow for the underwater environment is that the background removal methods applied on land are valid for this environment. Several recent phenomenology studies (e.g., MR-2409, MR-2412) have indicated that the seawater interaction with the transmitter field creates a background response that is more pronounced than that typically encountered on land. Specifically, these studies have shown a large background response that dominates the early time measurements <0.5 ms (see e.g., Billings, 2016). Our dynamic processing flow applies a continuous background removal using a detrend window length of N samples (N is dependent on sample rate and survey speed). This approach is effective for removing a background that is constant or that varies slowly with respect to the anomaly frequency. Implementing this approach, however, assumes that the background interaction with the target is negligible. Therefore, we want to demonstrate that the seawater and target interaction can be neglected for the measurement time gates of interest (i.e., 0.5 – 10 ms window after transmitter shutoff).

Data Requirements

We will use an electromagnetic simulation environment to assess the target and seawater interactions imparted by a transmitter coil sized comparably to the underwater sensor dimensions. We will investigate the free space (in-air) response of the target, the background response of the seawater and seafloor, and the combined response of the target embedded in the seawater and seafloor environment.

Metric

This objective uses a background response metric that compares the response of the target in air (R_T^{air}) to the response of the seawater and seafloor background (R_B^{sea}) subtracted from the response of the target embedded in the seawater/seafloor environment (R_T^{sea}).

Success Criteria

For our background removal approach to be valid, we need $R_T^{air}(t_n) \approx R_T^{sea}(t_n) - R_B^{sea}(t_n)$ for 0.5 ms $< t_n < 10$ ms.

3.5 OBJECTIVE: ORIENTATION STABILITY

Given the relatively close proximity of the sensor to the seafloor (we target a nominal 1.0-meter standoff for operation), large changes in sensor angle (particularly roll angle) could result in an undesired contact with the seafloor. Additionally, we expect that large changes in pitch or roll angle (with respect to the seafloor) will create variation in the background response. Slowly varying background changes should be managed by the background removal process (see Objective 3.4); nonetheless, we want to minimize any background variability as much as possible. Therefore, an array that maintains a stable orientation with respect to the seafloor is desired for effective operation.

Data Requirements

We will apply a hydrodynamic simulation environment to assess the pitch and roll response of the array to an initial perturbation.

Metric

This objective uses the predicted pitch and roll response as a function of time to assess performance.

Success Criteria

We consider a sensor array that settles to within +/- 5 degrees of horizontal after an initial perturbation to be stable.

3.6 OBJECTIVE: POSITION STABILITY

For effective survey line following, we want to ensure that the array will maintain a steady course. Any tendency for lateral position drift is undesirable. Additionally, a stable vertical position is also desired to maintain fixed seafloor standoff (see Objective 3.5). Accordingly, lateral and vertical position stability will be important for effective survey operations.

Data Requirements

We will apply a hydrodynamic simulation environment to assess the heave and sway response of the array to an initial perturbation.

Metric

This objective uses the predicted heave and sway response as a function of time to assess performance.

Success Criteria

We consider a sensor array that settles to within 0.5m lateral offset and to within 0.15m vertical offset from neutral position after an initial perturbation to be stable.

3.7 OBJECTIVE: STANDOFF STABILITY

As discussed in 3.6 and 3.7, maintaining constant standoff above the seafloor is desired for operation and background consistency.

Data Requirements

We will apply a hydrodynamic simulation environment to assess the heave motion during operation in worst case surface conditions (Sea State 3).

Metric

Standoff stability will be determined by evaluating the heave response to perturbations imparted by surface conditions.

Success Criteria

Maintaining seafloor standoff within +/- 0.15m of neutral will indicate success.

3.8 OBJECTIVE: DEPTH CONTROL RESPONSIVENESS

Because the winch pay-in/pay-out controls the depth, and therefore, seafloor standoff of the array, we want the responsiveness of the system to be sufficient for following changes in seafloor slope.

Data Requirements

We will apply a hydrodynamic simulation environment to assess the vertical velocity of the array in response to winch pay-in at different tow speeds.

Metric

We will consider the vertical velocity in relation to the survey speed (forward velocity).

Success Criteria

We desire the array to be responsive enough to adjust to changes in seafloor slope of up to 10% (e.g., 0.1 m/s vertical velocity at 1.0 m/s forward velocity).

3.9 OBJECTIVE: OPERATING LOAD FEASIBILITY

We want to ensure that the operating loads encountered under typical survey conditions will be well within the safety factor and operational limits of standard, commercially available tow hardware (winch and towline).

Data Requirements

We will apply a hydrodynamic simulation environment to evaluate worst case limits for towline tension.

Metric

We will evaluate towline tension to assess feasibility.

Success Criteria

Towline tension should fall within specifications of standard tow components.

3.10 OBJECTIVE: EFFECTIVE TARGET LOCATION TRACKING

Our final performance objective combines the hydrodynamic performance with EMI classification performance. We will assess the cumulative position errors due to sensor array tracking error and target location estimation error.

Data Requirements

We will use the hydrodynamic simulation environment as well as EMI data to identify the expected errors due to target estimation from data inversion and array location error due to kinematic transformation.

Metric

We will evaluate the overall target location error.

Success Criteria

We consider target location error $<0.5\text{m}$ to be sufficient for anomaly detection and reacquisition.

Page Intentionally Left Blank

4.0 TEST DESIGN

To assess the performance metrics, our test design comprised experimental and simulation components. The simulation included a hydrodynamic modeling environment and an electromagnetic modeling environment. The first stage of our analysis was to assess the EMI-based classification performance of the sensor design using our EMI design simulator. Validation of EMI model predictions compared predicted polarizabilities to those acquired from experimental test stand data collection. After confirming EMI-based classification performance, we then moved the concept to the hydrodynamic simulation environment. During this stage, we evaluated the hydrodynamic stability of the sensor design under the anticipated range of survey conditions.

4.1 EMI TEST DESIGN

Our EMI design simulator runs in the Matlab environment and incorporates the models we use for advanced classification processing. The basis for the simulator is a forward model that calculates the transmitter magnetic field intensity and direction corresponding to the size, shape, orientation, number of windings, and current specified by the user for each of the selected transmitter coils entered in the design. The user also selects a TOI type, location, and orientation using a Cartesian coordinate frame centered at the sensor location and a set of Euler rotation angles defined with respect to this frame.

The response of the TOI to each transmitter field is generated using a dipole model with electromagnetic polarizabilities defined by the appropriate TOI library (i.e., the one selected by the user). Dipole moments are created along each of the principal axes of the TOI using these polarizabilities and the projection of the transmitter fields on each principal axis of the TOI. The dipole moments create a secondary magnetic field (TOI response) that is then calculated at the user specified receiver locations. Secondary field values are created for each time gate in the TOI library to produce time-dependent, synthetic data at each receiver location.

The key to effective classification is to resolve each of the three principal TOI polarizabilities by inverting the data (i.e., the reverse of the forward model process just described, that is to use the data to identify the TOI properties). The forward/inverse process can be summarized by the following equation:

$$[dataX \ dataY \ dataZ] = [L1 \ L2 \ L3] \begin{bmatrix} T11 & T12 & T13 \\ T21 & T22 & T23 \\ T31 & T32 & T33 \end{bmatrix} \quad (4.1)$$

The left side of Equation 4.1 represents the (x, y, z) components of the magnetic field data (either real or synthetic) measured at a receiver. The 1×3 L -matrix represents the three principal polarizabilities of the target and the 3×3 T -matrix contains the dipole terms associated with the target location, orientation, and transmitter field projection on the target principal axes. For the inversion process, once the optimal T -matrix is determined, the three polarizabilities can be resolved.

Because each principal polarizability contributes to each component of the data, it is possible to encounter scenarios where it is difficult or impossible to resolve a polarizability even if the data appear to maintain a relatively high signal-to-noise ratio. For example, consider the $L2$ polarizability.

The $L2$ contribution to the data consists of the three terms: $L2*T21$, $L2*T22$, $L2*T23$. If all three of these terms are below or close to the typical noise standard deviation encountered in the data, the $L2$ polarizability cannot be sufficiently or reliably resolved. That is:

$$L2*T21, L2*T22, L2*T23 \approx \sigma \quad (4.2)$$

where σ represents the noise standard deviation. Consequently, if a particular target location or orientation produces low values for the $T21$, $T22$, and $T23$ elements, it may be difficult or impossible to resolve the $L2$ polarizability if noise levels are sufficiently high. Therefore, understanding the noise characteristics of a sensor is critical to estimating its classification performance.

Creating representative synthetic data requires the addition of noise to the forward model output. As discussed, the characteristics of the noise will, under certain conditions, determine whether each principal polarizability can be resolved from inversion. Our approach to creating noise is to replicate the noise characteristics recovered from actual sensor data. One method is to apply the standard deviation observed in real data to normally distributed synthetic noise. For example, we can measure the standard deviation for N samples measured in the i^{th} receiver channel at the j^{th} time gate. We can subsequently apply this standard deviation to scale M samples of normally distributed synthetic noise, which is then added to the corresponding channel in the forward model output:

$$D_{ij}(m=1:M) = F_{ij} + \sigma_{ij}*Ns(m=1:M) \quad (4.3)$$

Here, D_{ij} is the synthetic data corresponding to the i^{th} receiver channel at the j^{th} time gate; F_{ij} is the forward model output corresponding to this same receiver channel and time gate; σ_{ij} is the standard deviation of the noise measured over N samples of data acquired at this channel and time gate; and Ns is normally distributed random noise with standard deviation of 1. An example of this method is shown in Figure 9. This example shows the noise distribution for survey data and synthetic data.

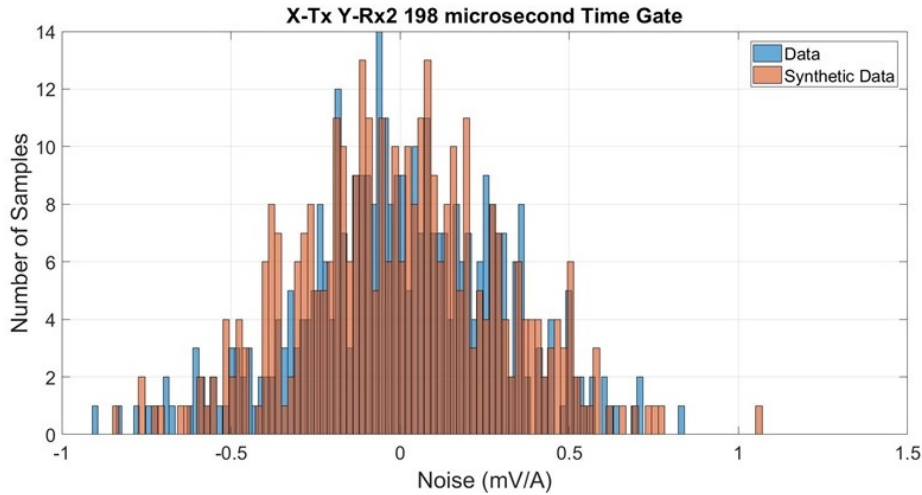


Figure 9. Example of Real and Synthetic Data Noise Characteristics.

This plot shows the noise distributions corresponding to 360 samples of data from the X-transmit Y-receiver channel at the 198-microsecond time gate.

While noise characteristics may change for different sensor configurations, we believe that using existing survey data is an effective way to replicate the typical noise characteristics of advanced EMI sensors. Additionally, we can apply survey specific noise types depending on the intended application of the sensor. For example, if we are trying to predict the performance of a dynamic survey sensor, we can apply the noise characteristics measured during dynamic surveys to produce synthetic data for the candidate sensor configuration. Dynamic survey data contain noise associated with movement of the sensor in addition to the baseline sensor and environmental noise.

For this design study, we developed the forward model for the 3D sensor array configuration shown in Figure 4. Figure 10 through Figure 13 show the forward model design parameters that describe the concept configuration.

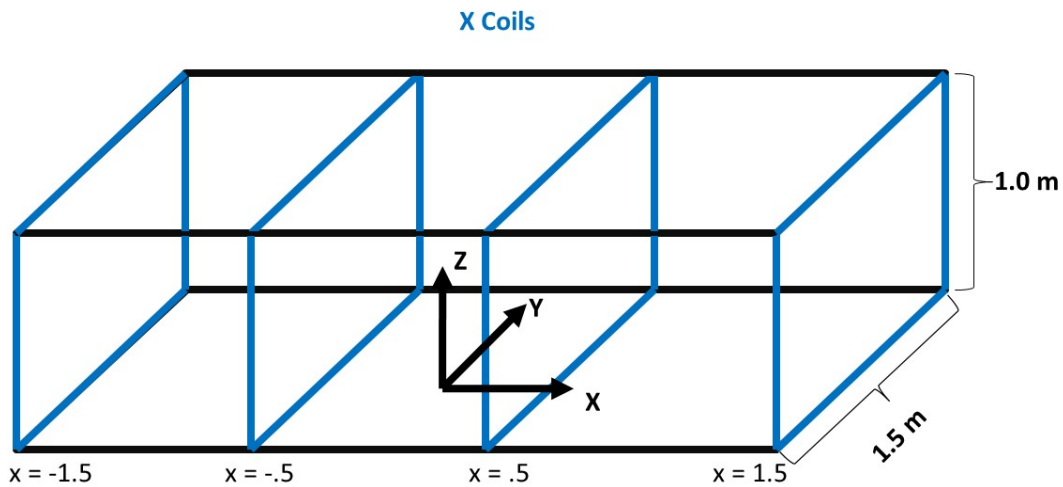


Figure 10. X-coil Design.

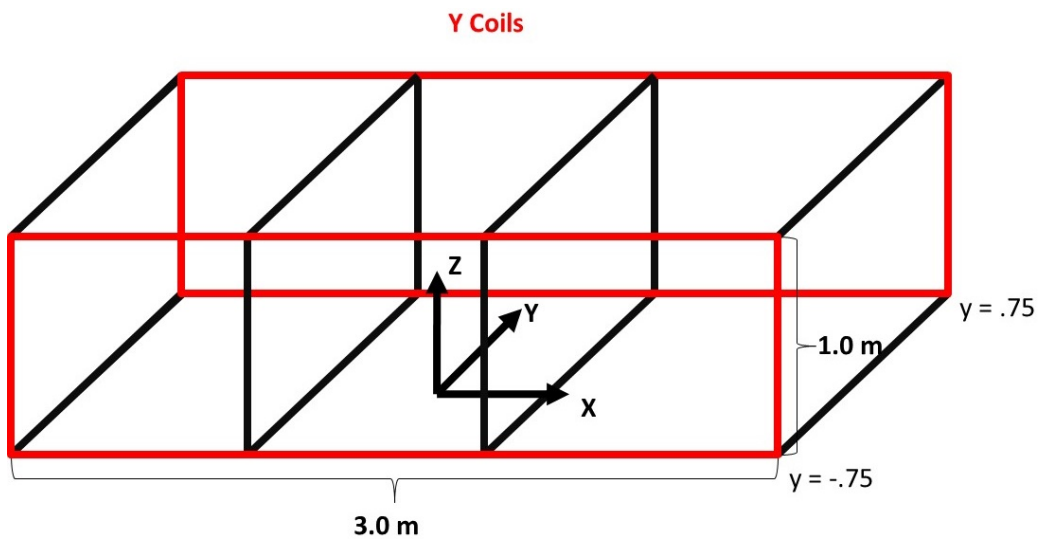


Figure 11. Y-coil Design.

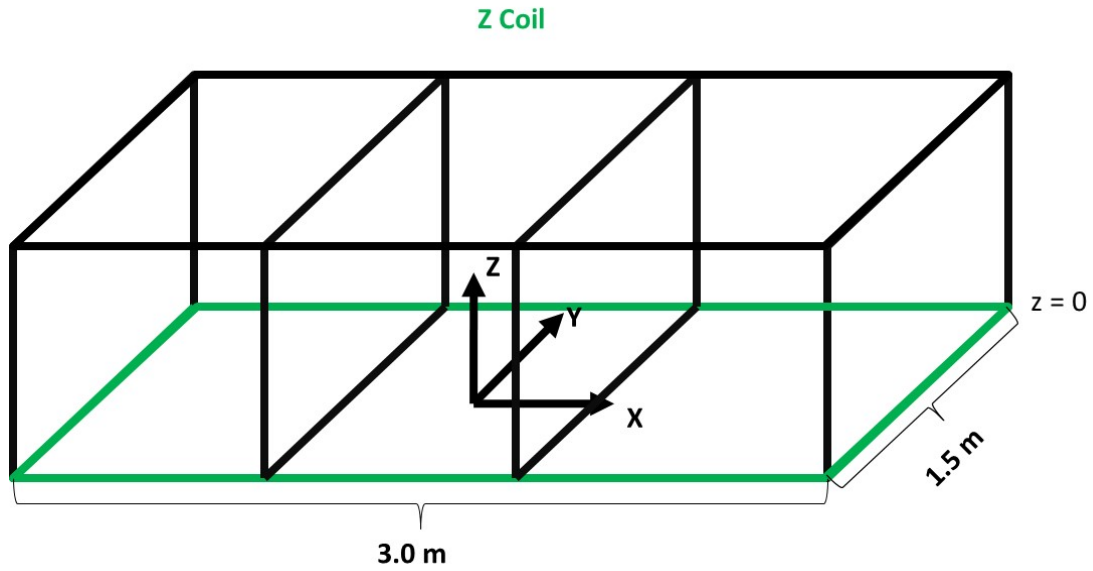


Figure 12. Z-coil Design.

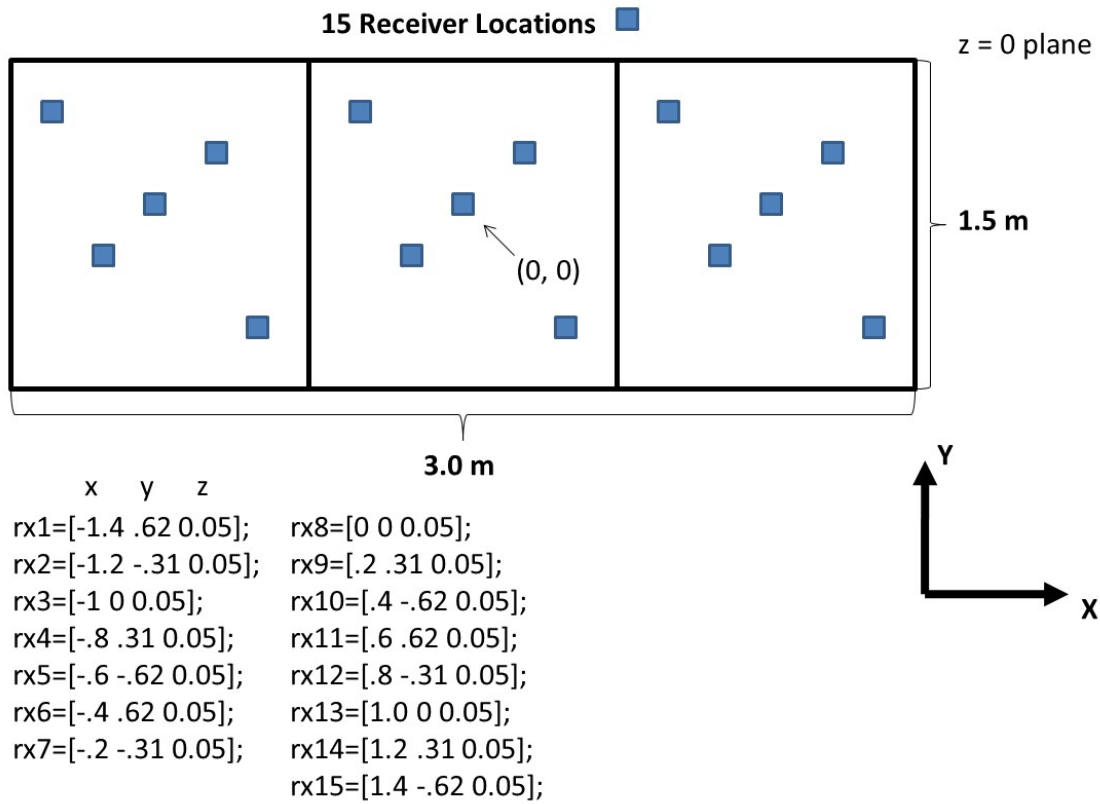


Figure 13. Receiver Locations.

After generating a forward model output for this configuration, we add noise to produce synthetic data. To assign noise characteristics to each receiver channel, we apply the standard deviation values measured in dynamic OPTEMA survey data. While the noise characteristics will likely be different in the underwater environment, we believe the dynamic OPTEMA data provide a relevant noise baseline since these data capture motion induced noise created by rotation of the receivers in the Earth's magnetic field, a condition that will be encountered to some extent underwater as well. Figure 14 shows the typical noise characteristics measured in dynamic survey data.

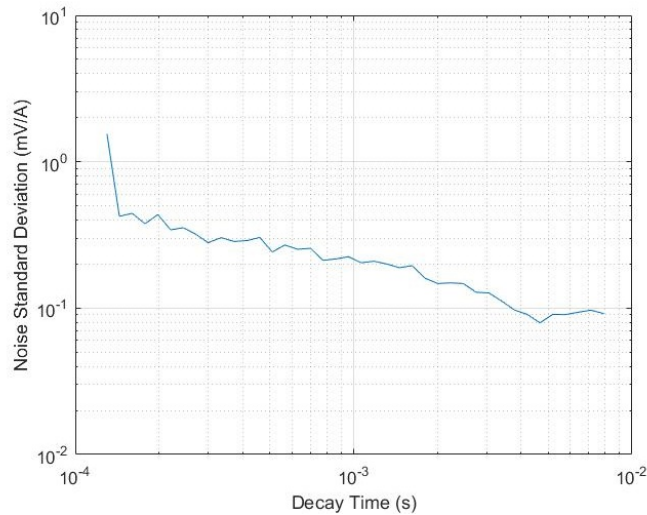


Figure 14. Typical Noise Standard Deviation Measured in Dynamic OPTEMA Survey Data.

We applied these characteristics to the forward model output for the towed array concept.

The forward model output combined with the dynamic noise characteristics provides the basis for simulating dynamic underwater towed array performance. Using this simulation environment, we can establish baseline performance against different TOI encountered in a variety of depths, across track offsets, and orientations.

4.2 HYDRODYNAMIC TEST DESIGN

The hydrodynamic performance of the towed EMI sensor array system was modeled by Dynamic Systems Analysis Ltd. (DSA) using their ProteusDS dynamic analysis simulation software package. We initially considered four different towing system designs: a direct tow system, a clump weight system, a passive depressor wing system, and an active depressor wing system. We down-selected to the clump weight system for the hydrodynamic performance analysis due to its relative simplicity in design and operation. The overall objective of the hydrodynamic analysis was to ensure that the towed sensor system design meets the following criteria:

- Towed EMI sensor body width: 3m
- Tow speeds: Operate in 3-4 knots
- Tow altitude: The towed sensor is to maintain a height above seabed of 1m (2m maximum)
- Water depth: Operate in depths of 10-30m

- Wave conditions: Operate in Sea state 3, $H = 1.25\text{m}$, $T=5$ second
- Stability: Maintain stability during turns and typical operating conditions
- Mechanical design: Ensure towline strength and winch capacity are sufficient to handle hydrodynamic loads induced by the towed EMI sensor system.

In the ProteusDS simulation, the towed EMI sensor is setup as a 6 DOF¹ rigid body with several surfaces that provide hydrodynamic loads and buoyancy force. The tow design incorporates a four-point bridle that extends from the clump weight and aids in yaw and pitch stability of the sensor. We selected a bridle length to create a 60-degree angle as DSA’s previous experience with towing bridles has demonstrated that a 60-degree bridle provides quick response to changes in tow direction. The tow points were chosen to be 1m from the center of the structure on both sides. The overall bridle length is 1.7m. The bridle configuration is shown in Figure 15.

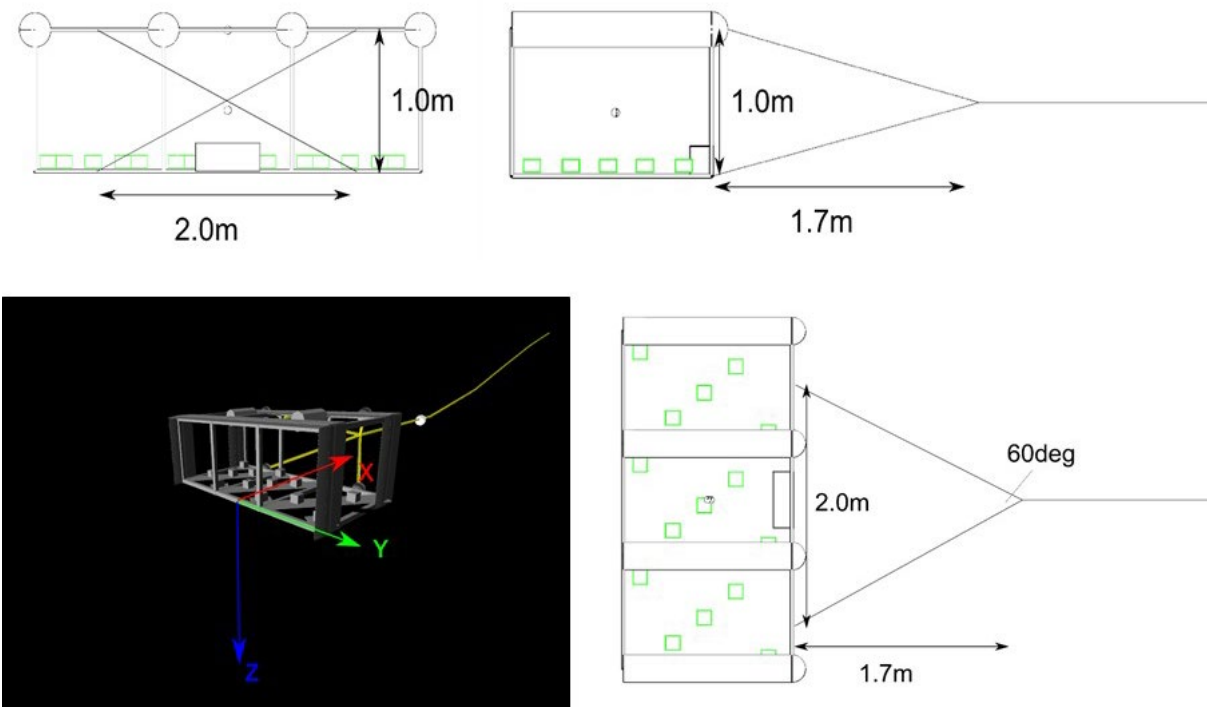


Figure 15. Proposed Bridle Configuration.

Note the X-, Y-, Z- reference frame shown here is different from that used for the EMI convention.

Sensor depth is determined by the layback and towline angle as shown in Figure 16. The towline angle is dependent upon the clump weight and drag force. For a fixed velocity, the winch controls the layback to adjust the sensor height above the seafloor. Figure 17 shows a free body diagram of the forces that determine the towline angle.

¹ 6 DOF: Surge, sway, heave, roll, pitch, yaw

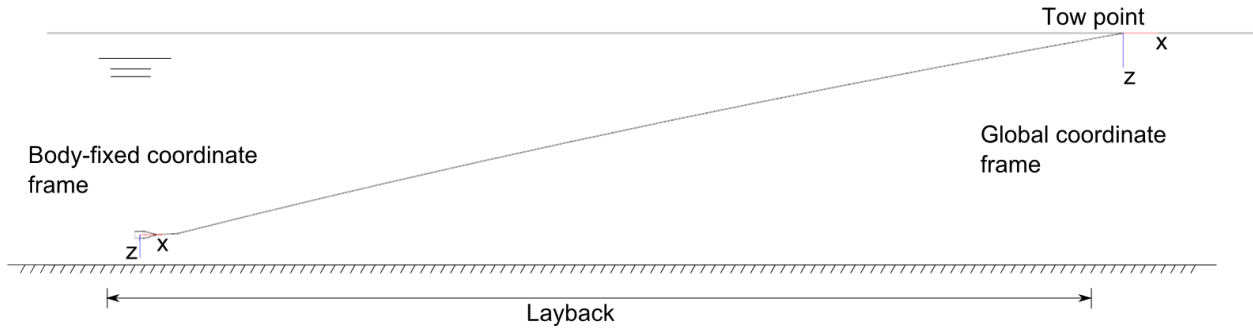


Figure 16. Towing System Global Frame and Body-fixed Coordinate Frame

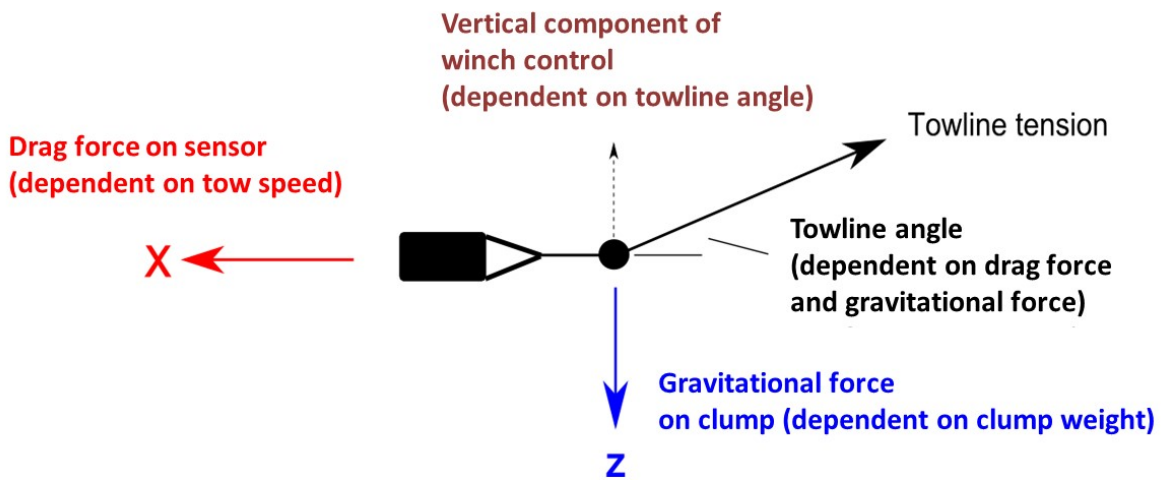


Figure 17. Free Body Diagram Illustrating the Forces Acting on the Tow Body System.

Winch pay-in/pay-out determines the sensor height above the seafloor for a fixed velocity.

Key input parameters to the hydrodynamic model are the mass and volume (buoyancy) of all tow body components. The total mass of the sensor in the analysis was estimated to be 359 kg. The mass of each component and the total mass of the structure are presented in Table 3.

Table 3. Towed EMI Sensor Mass Properties.

Transmitter mass / unit length:	7.2 kg/m
Transmitter mass (single beam: top, bottom):	22.1 kg each
Transmitter mass (single beam: front, back):	11.3 kg each
Transmitter mass (single beam: port, port-center, starboard-center, starboard):	7.7 kg each
Top plate (2x):	7.9 kg each
Side plate (4x):	2.5 kg each
Receivers (15x):	2.0 kg each
Receiver base plate:	43.0 kg
Electronics (2x):	10.0
Total mass:	359.3 kg
Center of gravity – x:	0.785 m
Center of gravity – y:	0 m
Center of gravity – z:	-0.489 m
Moment of inertia – x:	99.7 kg*m ²
Moment of inertia – y:	244.9 kg*m ²
Moment of inertia – z:	70.2 kg*m ²

The towed EMI sensor is modeled as positively buoyant, with a net buoyancy of 4.7kg. To determine this net buoyancy, the buoyancy force of each component is calculated using the displaced volume. The principal dimensions of each component and the total volume can be found in Table 4. The total buoyancy of the towed EMI sensor (excluding the bridles and clump) is 364kg. The mass of the towed EMI sensor is 359.3 kg, which produces a net positive buoyancy of 4.7 kg.

Table 4. Component Principal Dimensions and Total Volume.

Component:	X dimension (m):	Y dimension (m):	Z dimension (m):	Total volume (m³):
Transmitter beam (3m)	0.06	3.07	0.06	1.10x10 ⁻²
Transmitter beam (1.5m)	1.57	0.06	0.06	5.62x10 ⁻³
Transmitter beam (1.0m)	0.06	0.06	1.07	3.83x10 ⁻³
Receiver	0.13	0.13	0.13	2.05x10 ⁻³
Electronics cylinder	0.5	0.24	0.24	2.26x10 ⁻²
Top plate	0.3	3.07	0.05	4.14x10 ⁻²
Side plate	0.3	0.04	1.07	1.28x10 ⁻²
Base mount (with gaps)	1.57	3.07	0.01	2.58x10 ⁻²

With the basic input parameters identified, we selected several load cases to evaluate the towed EMI sensor hydrodynamic performance under expected operating conditions. Specifically, we assessed three criteria: stability, control, and operability. The load cases selected to test the towed system for each criterion are listed in Table 5.

Table 5. Simulated Load Cases for the Hydrodynamic Performance Assessment.

Category	Sub-Category	Test	Test Number	Comments
Stability Load Cases				
	Towed EMI sensor righting moment			Array only, no towline. Initial roll/pitch offset.
		Roll	S-01	
		Pitch	S-02	
	Transient response			Towline present, yaw/heave offset.
		Sway	S-03	
		Heave (falling)	S-04	
		Heave (rising)	S-05	
	Wave response			Wave test cases, both wave encounter frequencies.
		Sea state 3 - opposing	S-06	Height: 1.25m Period: 5.0sec
		Sea state 3 - with	S-07	Height: 1.25m Period: 5.0sec
	Cross current			Platform stability and sway position in 0.5 m/s and 1 m/s cross current
		0.5 m/s	S-08	
		1 m/s	S-09	
Control Load Cases				
	Winch response			Determine towed EMI sensor heave response to winch control
		1.0 m/s tow speed, 25kg clump weight	C-01	
		1.0 m/s tow speed, 50kg clump weight	C-02	
		1.0 m/s tow speed, 75kg clump weight	C-03	
		1.5 m/s tow speed, 25kg clump weight	C-04	
		1.5 m/s tow speed, 50kg clump weight	C-05	
		1.5 m/s tow speed, 75kg clump weight	C-06	
		2.0 m/s tow speed, 25kg clump weight	C-07	
		2.0 m/s tow speed, 50kg clump weight	C-08	
		2.0 m/s tow speed, 75kg clump weight	C-09	

**Table 5. Simulated Load Cases for the Hydrodynamic Performance Assessment.
(Continued)**

Category	Sub-Category	Test	Test Number	Comments
Operating Load Cases				
	Operating configurations			Determine loads and layback on the system during normal towing operations
		Tow speed 1 knot	O-1	
		Tow speed 2 knot	O-2	
		Tow speed 3 knot	O-3	
		Tow speed 4 knot	O-4	
	Turning			Determine array stability when turning
		Turning - 1	O-5	
	Start/stop			Determine towed EMI sensor reaction on start up or sudden stop
		Sudden stop	O-6	
		Start up	O-7	

These load cases form the basis for our hydrodynamic performance assessment. We assessed the results of each load case using the hydrodynamic performance metrics discussed in Section 3 to determine the overall feasibility of the towed array concept.

5.0 PERFORMANCE ASSESSMENT

Our performance assessment consisted of two stages: 1) verification of EMI classification performance; and 2) verification of towed operation feasibility. The classification performance assessment comprised test stand data collection to verify the EMI modeling process, followed by simulations to determine expected classification performance as a function of target type and range. The towed operation assessment included simulations of the hydrodynamic load cases in the ProteusDS environment. Throughout both stages we applied the performance metrics described in Section 3 to determine whether the specific performance objectives were met. Details of the assessment and the performance objective results are presented in the following subsections.

5.1 OBJECTIVE: MODEL ACCURACY

We fabricated a 2/3-scale mockup of the towed EMI array concept that we used to verify the model accuracy. The mockup comprised 1 Z-coil (vertical), 2 Y-coils (along track), and 3 X-coils (across track) and 10 3-axis receiver cubes as shown in Figure 18. The OPTEMA transmitter module provided the drivers for the 3 sets of transmitter coils.



Figure 18. A 2/3-scale Mockup of the Underwater Towed Array Concept.

The array comprises 1 Z-directed transmitter, 2 Y-directed transmitters, 3 X-directed transmitters, and 10 receiver cubes.

The first step in model verification was to capture the noise characteristics of the mockup system. We measured the standard deviation of static test stand data at all time gates (out to 8.3 ms) for each of the 90 receiver channels. We then applied these standard deviation values to create synthetic noise for the forward model output (after modifying the forward model to include the mockup configuration parameters). Figure 19 shows the noise standard deviation values calculated for test stand and model data.

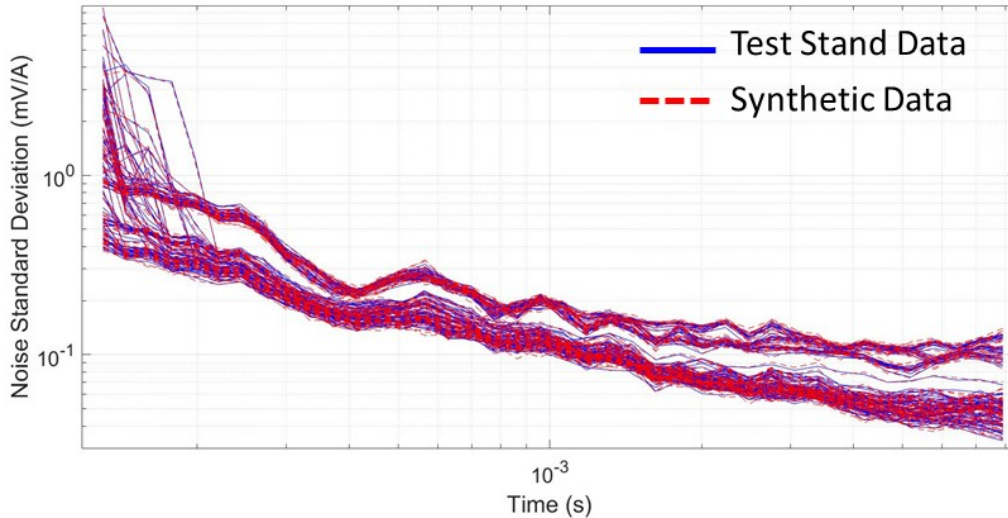


Figure 19. Noise Standard Deviation Values Corresponding to 90 Receiver Channels as a Function of Time Gate (Horizontal Axis).

Each line represents a single receiver channel. Standard deviation values were calculated for 400 samples of test stand data (blue) and synthetic data (red).

To test the model accuracy, we acquired static, grid-based data over a 60-mm projectile (Figure 20). Our objective was to collect data at grid locations that would provide full constraint of the three polarizabilities (i.e., good classification) as well as at grid locations that did not constrain all three polarizabilities (i.e., poor classification). These two scenarios would establish whether the model could accurately predict grid locations where classification was not reliable.



Figure 20. Grid-based Test Stand Data Collection.

We used a 60-mm test object placed at various X-Y-Z grid coordinates to identify locations that provided high quality classification and locations that provided unreliable classification.

For each grid location tested, we ran the simulation with the 60-mm target in the corresponding location in the model. We then inverted the synthetic data with sensor noise added to obtain the polarizabilities. To compare the model performance to the test stand sensor, we used a library match metric that calculated the fit between the polarizabilities (from both real and synthetic data) and the relevant 60-mm TOI library.

This library match metric was originally developed for OPTEMA dynamic data and was tested on the Southwestern Proving Ground data set. The match metric determines a fit between each test polarizability (i.e., derived from inversion of the data) and the corresponding library polarizability:

$$f = \frac{\sum_{i=1}^N |L(t_i)_{lib}^{1/2} - L(t_i)_{test}^{1/2}|}{\sum_{i=1}^N L(t_i)_{lib}^{1/2}} \quad (5.1)$$

Here L is the polarizability. A fit, f , is generated for each of the three polarizabilities. The match metric is a weighted sum of the three fits. The N th time gate can be adjusted to reflect earlier or later portions of the decay. For the OPTEMA dynamic data, the match metric incorporated the highest fit value for each polarizability within the cluster. Figure 21 shows the results of applying this match metric to OPTEMA data collected at the Southwestern Proving Ground.

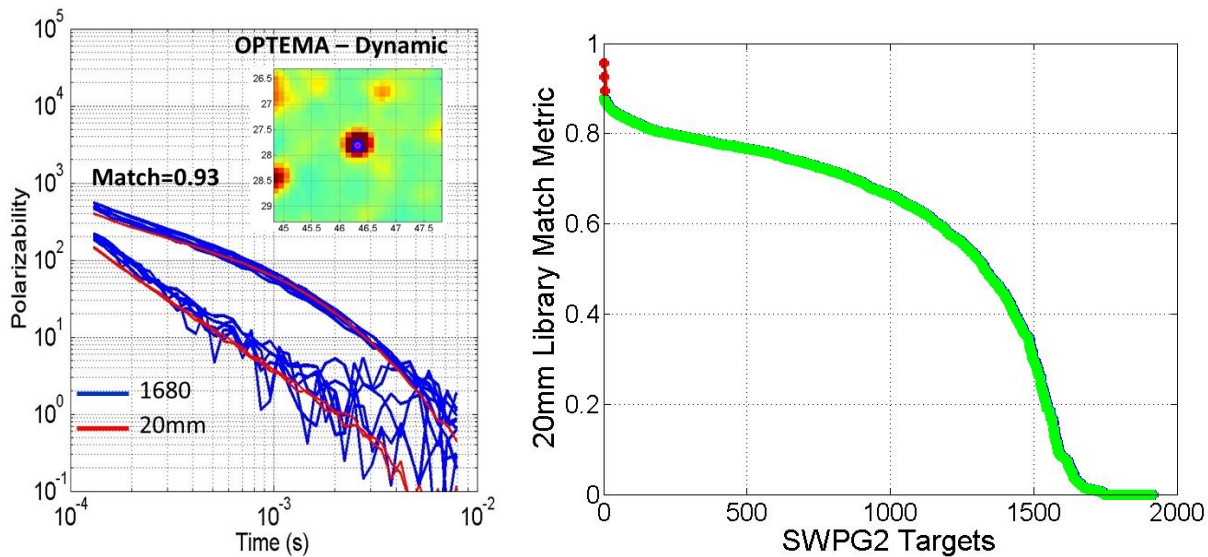


Figure 21. LEFT: Library Match Metric Applied to OPTEMA SWPG Data from a 20mm Projectile Encounter. RIGHT: Library Match Metric Applied to Approximately 2000 Anomaly Encounters at Southwestern Proving Ground.

Red corresponds to 20mm TOI. Green corresponds to clutter items.

For 30 grid locations tested, the library match generated from the model data was within 5% of the library match generated from the test stand data. The model results agreed with test stand results even for cases where polarizabilities were not well constrained. These results indicate that the model can accurately predict scenarios where classification will be sub-optimal. Figure 22 shows the measured and predicted match values for the different grid locations. Figure 23 and Figure 24 show specific examples where the model and data agree on well-constrained and poorly-constrained scenarios.

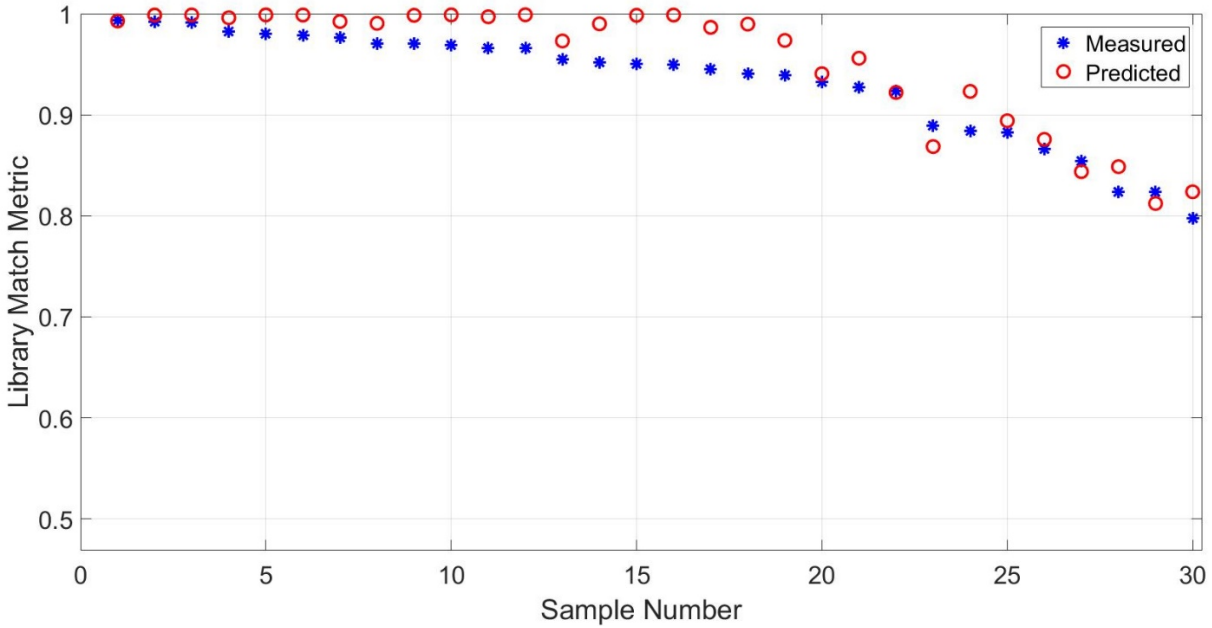


Figure 22. Library Match Metric for 30 Grid Locations.

The results show agreement between measured (test stand) and predicted (model) polarizability matches. It is important that the model is able to accurately predict cases where polarizabilities are not well constrained, i.e., for match values <0.9.

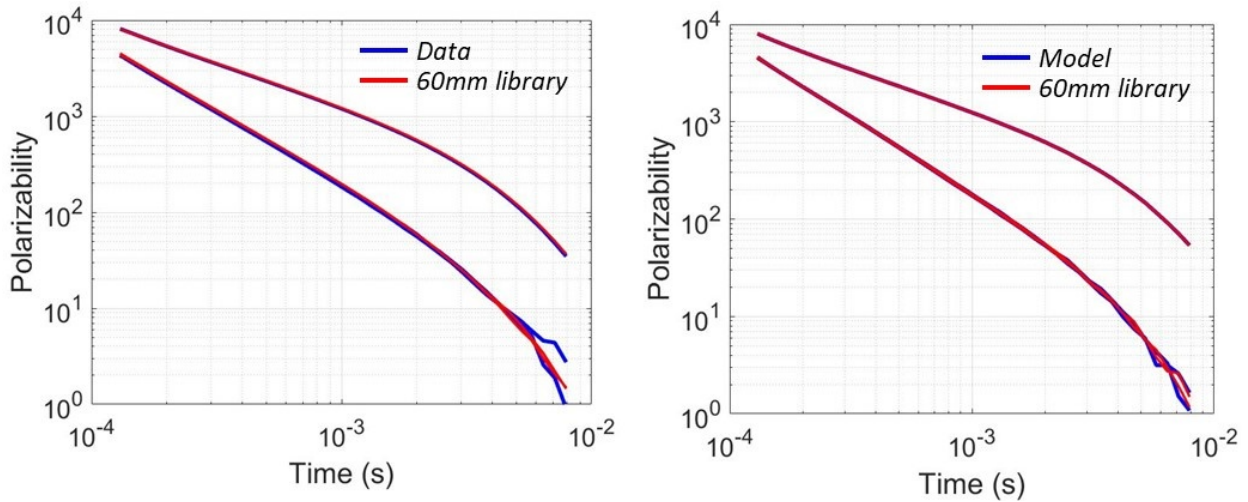


Figure 23. Example of Well Constrained Polarizabilities.

Here the data (left) and model (right) both show similar high-quality match.

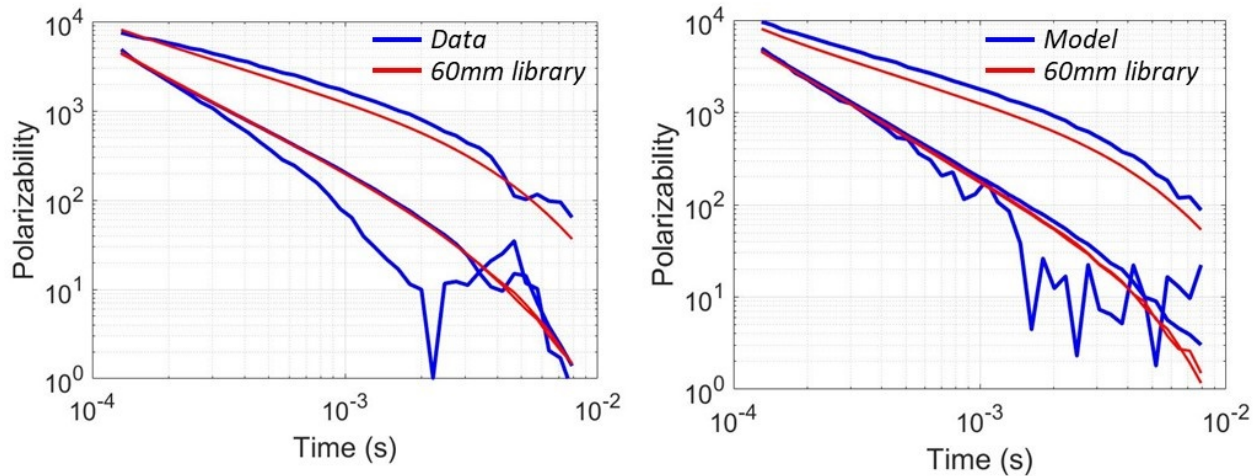


Figure 24. Example of Poorly Constrained Polarizabilities.

Here the data (left) and model (right) both show a similar low-quality match.

5.2 OBJECTIVE: EFFECTIVE EMI SENSOR CONFIGURATION

One of the fundamental requirements for an underwater towed array is that the sensor can perform optimally at significantly higher standoffs than those typically required for land surveys. Our initial design assumption for the dynamic towed sensor is that standoff above the sea floor will be, at a minimum, 1 meter. Therefore, one of the key design drivers was to develop a transmitter configuration that would provide the required field uniformity necessary for reliable classification at depths of 1 meter or more below the sensor. This requirement differs significantly for land-based sensors that are typically optimized for classification in the 0 – 1 meter depth range.

The starting point for our design study was the OPTEMA sensor configuration, which we demonstrated can provide effective dynamic classification in the 0 – 1 meter depth range. We modified this 3D transmitter configuration by extending the footprint from 1 meter x 2 meters (for the OPTEMA) to 1.5 meters x 3 meters for the underwater configuration. We also changed the orientation of the vertical transmitters and added two more across-track vertical transmitters in series. These changes are summarized in Figure 25.

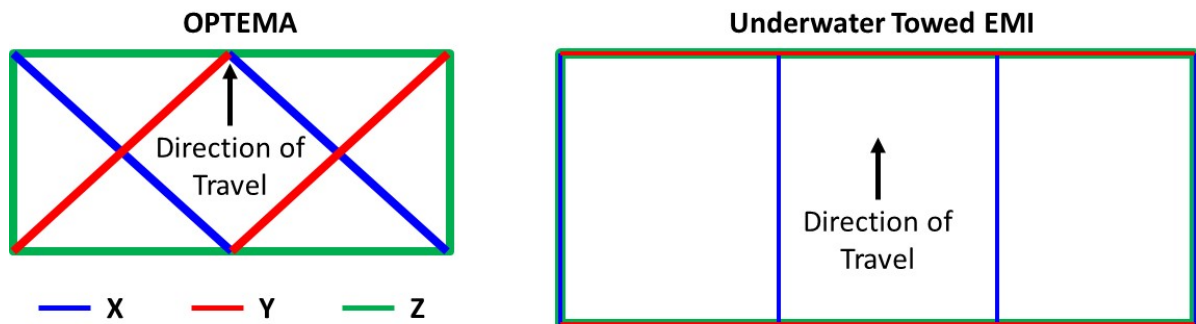


Figure 25. Diagram of Modifications Made to OPTEMA Design for the Underwater Towed Configuration.

We selected this design due to the magnetic field distribution at depths greater than 1 meter. While the spacing of the transmitters creates non-uniform regions at different across track locations for depths that are <0.5 meters, the across-track uniformity at depths >1 meter for all three transmitter axes will ensure full constraint of polarizabilities for any target encounters at those depths. The non-uniformities in close proximity to the sensor create “blind spots” where the data SNR remains high, but the polarizabilities are not well constrained (Figure 26).

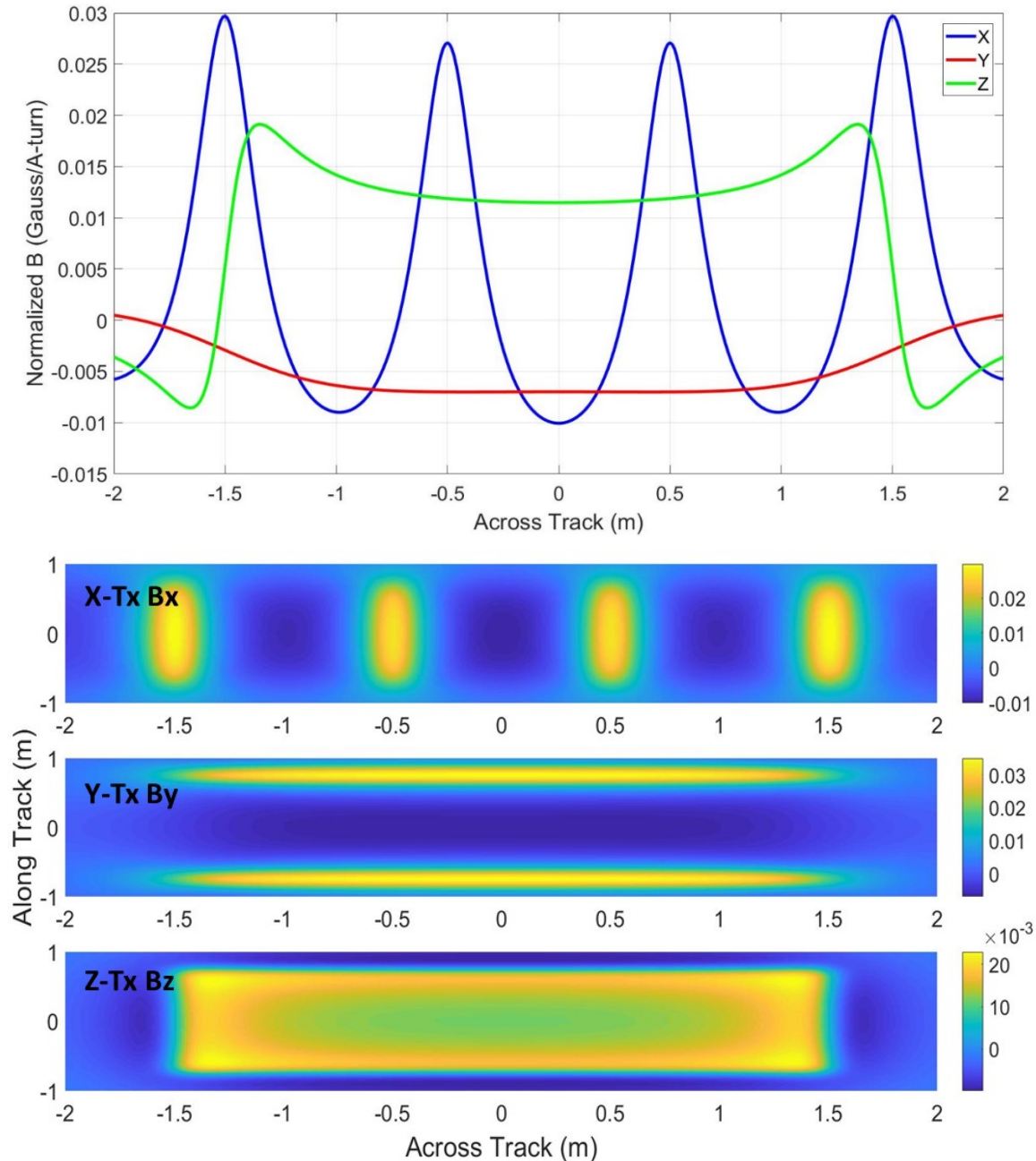


Figure 26. Transmitter Field Principal Component Distributions 15 cm Below the Sensor.

The map view shows the location of several blind spots corresponding to the light blue regions within the sensor footprint.

These blind spots were evident during our test stand grid measurements when we encountered several grid locations where the polarizabilities did not provide a good library match despite high SNR (see, e.g., Figure 24). While SNR decreases at greater depths from the sensor, the blind spots disappear, making it possible to accurately recover the polarizabilities (Figure 27).

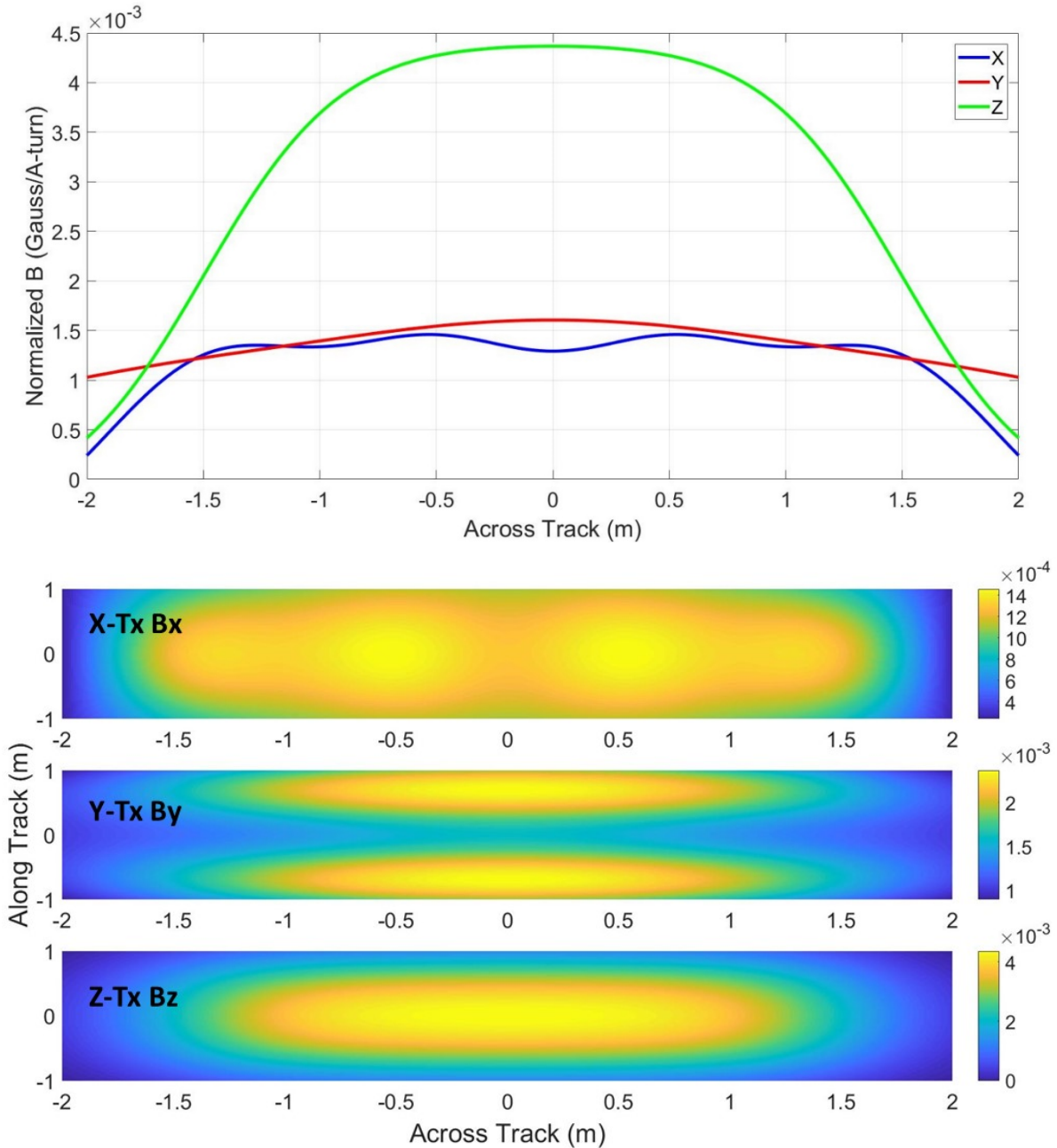


Figure 27. Transmitter Field Principal Component Distributions 1.0 m Below the Sensor.

At this depth all three principal components are uniformly distributed across track.

To test our design concept, we performed a series of simulated dynamic target encounters. Using the EMI forward model and dynamic noise characteristics captured from OPTEMA surveys, we simulated sensor overpass of TOI ranging in size from 81-mm projectiles to 155-mm projectiles at depths of 1 meter to 2.4 meters below the array. For each TOI/depth combination, we also varied across track target location between -1.6 meters to 1.6 meters (approximate swath of the sensor). Figure 28 shows a diagram of the simulation approach.

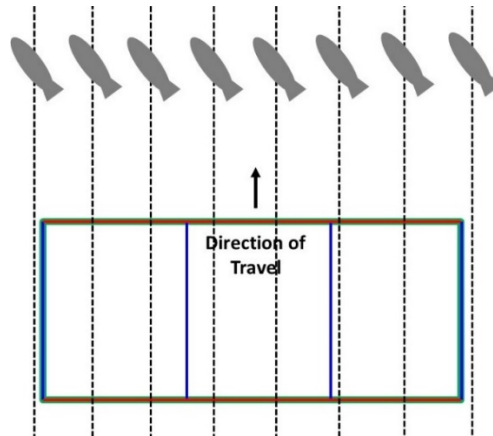


Figure 28. Diagram of Simulation Design.

We simulated target encounters at different across track locations across the full sensor swath. Each encounter placed the target at a unique depth, across track location, and orientation.

For each simulated encounter, we created synthetic data for array locations that were between +/-10 meters along track from the target position (20-meter line length total). We used sample spacings of 10 – 20 cm (simulating approximately 2-4 knots). We applied dynamic processing to each of these synthetic data lines that included a smoothing filter to reduce high frequency noise. After filtering, we inverted all soundings that were within +/-0.8 meters along track from the anomaly peak to produce a polarizability cluster. Figure 29 and Figure 30 show examples of synthetic dynamic data results.

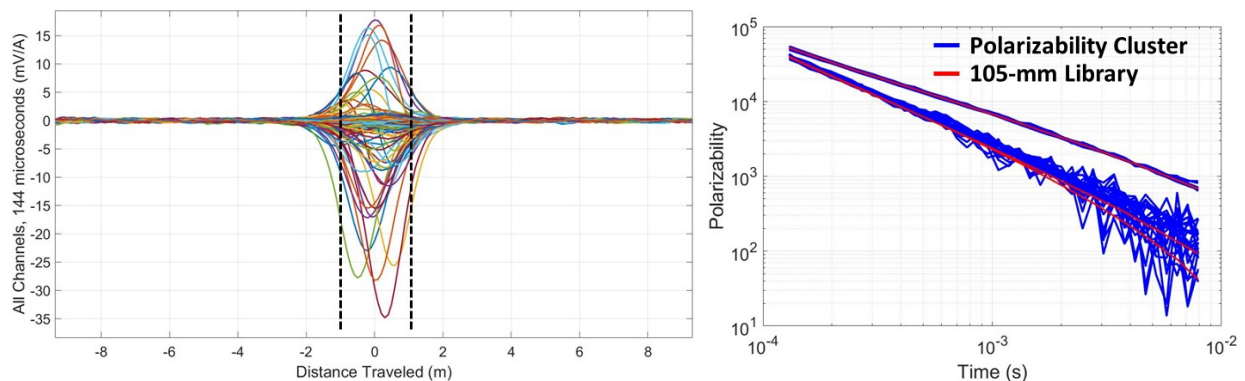


Figure 29. LEFT: Synthetic Dynamic Data Corresponding to 105-mm Projectile Encounter at 1-meter Depth.

All receiver channels are shown at the 144-microsecond time gate. The black dashed lines show the selection of soundings used for inversion. RIGHT: Polarizability cluster from synthetic data soundings compared to 105-mm library.

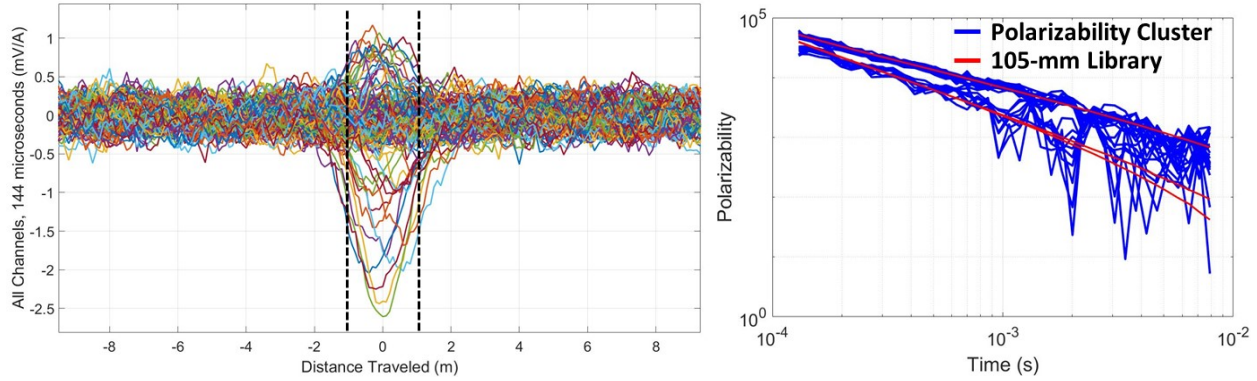


Figure 30. LEFT: Synthetic Dynamic Data Corresponding to 105-mm Projectile Encounter at 1.8-meter Depth. RIGHT: Polarizability Cluster from Synthetic Data Soundings Compared to 105-mm Library.

Left: All receiver channels are shown at the 144-microsecond time gate. The black dashed lines show the selection of soundings used for inversion. Right: The polarizabilities are noisy, but are still well constrained.

We ran approximately 250 simulations for the three TOI (81-mm, 105-mm, and 155-mm). Polarizability clusters from each simulation were compared to the appropriate library to determine a library match value. These values are shown in Figure 31.

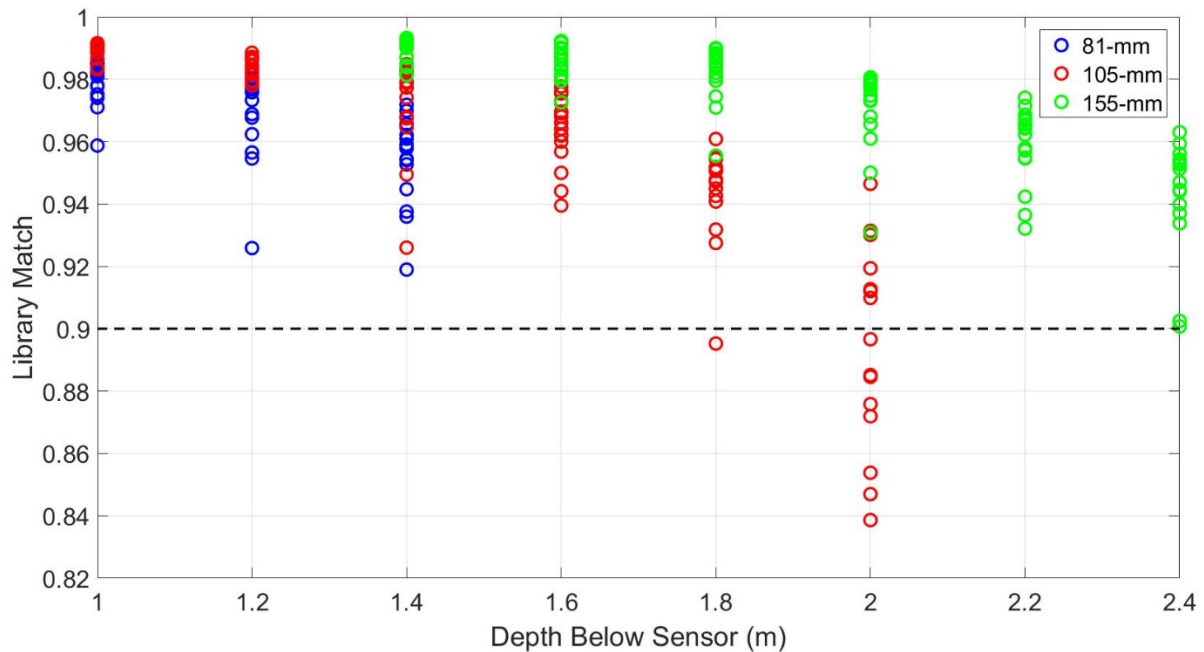


Figure 31. Library Match Results from 250+ Simulations of Dynamic Encounters with Three TOI.

The 0.9 match threshold represents the performance objective.

The results from these simulations indicate that it will be possible to recover high quality classification features from objects that are 1 meter or deeper than the sensor bottom. Our 0.9 match threshold showed that the 105-mm encounters started to produce high noise levels in the polarizabilities at depths of 1.8 – 2 meters while the 155-mm encounters started to produce high noise levels at 2.4-meter depths and beyond. We tested the 81-mm to a depth of 1.4 meters, maintaining high enough SNR to produce match values above 0.9.

One notable design consideration is that throughout these simulations we doubled the effective transmitter power from the baseline of approximately 100 A-turns used for OPTEMA to 200 A-turns. We anticipate that it will be necessary to use a higher power transmitter driver (i.e., one capable of greater voltage kickback levels) for the underwater towed sensor; however, these power levels should be obtainable without significant hardware redesign.

5.3 OBJECTIVE: EFFECTIVE UNDERWATER DYNAMIC CLASSIFICATION

The single shot dynamic classification approach discussed in Section 2.1 requires minimal position tracking of the sensor to produce reliable results; however, it can compensate for the movement of the sensor during the three transmit cycles within each sounding. As an example, consider the sensor movement at a speed of 3 knots, which is approximately 1.5 m/s. The sensor sample rate is 10 Hz, meaning a complete transmit cycle is performed over 15cm. For the three transmitter firings within the cycle, the sensor moves approximately 5 cm between each.

To assess the potential influence of position errors at the anticipated tow speeds, we acquired dynamic test stand data with the mockup and created intentional position errors in the data. For our experimental setup, we used a 155-mm projectile towed underneath the sensor at a depth of 1 meter. This process simulated dynamic overpass of the sensor array at tow speeds of 1-3 knots. During the dynamic data processing stage, we introduced position errors by modifying the sensor displacement measurement between each sample. We then inverted the data for polarizability clusters (Figure 32).

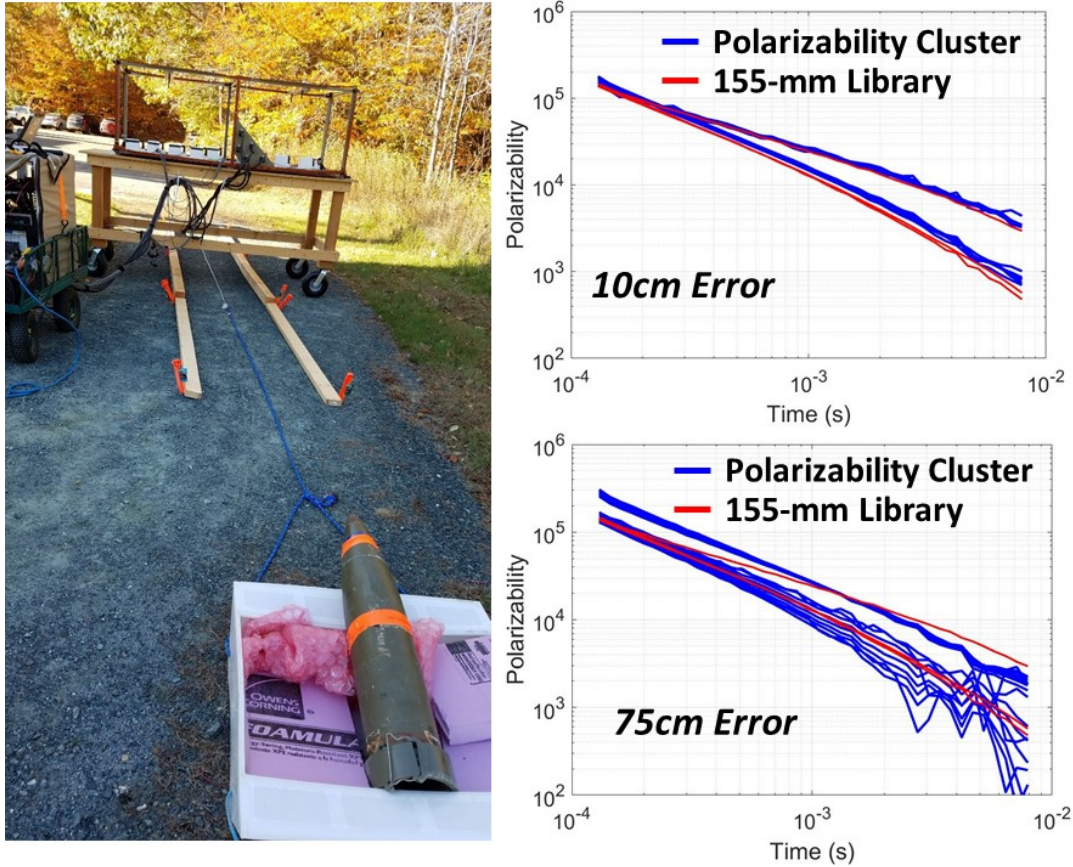


Figure 32. LEFT: Simulated Dynamic Towed Overpass for a 155-mm TOI Encounter. TOP RIGHT: Inversion Results for the Dynamic Test Stand Data with 10cm Position Error added. BOTTOM RIGHT: Inversion Results for the Dynamic Test Stand Data with 75cm Position Error Added.

Top Right: The polarizability cluster still provides a good library match. Bottom Right: The polarizability cluster no longer matches the 155-mm library.

The sensor displacement measurement between each sample allows the forward model to correct for the small displacement of the sensor between each of the three transmitter firings (typically on the order of 2-5 cm). For land surveys, this displacement is tracked using GPS. For our test stand data, we measured the average speed of the 155-mm during the encounter to determine the sensor displacement between each transmitter firing. We then increased or decreased the displacement input to the forward model to introduce position errors. For each amount of error, we calculated the library match to the 155-mm library that resulted from the data inversion. Figure 33 shows the resulting library match values as a function of added position error.

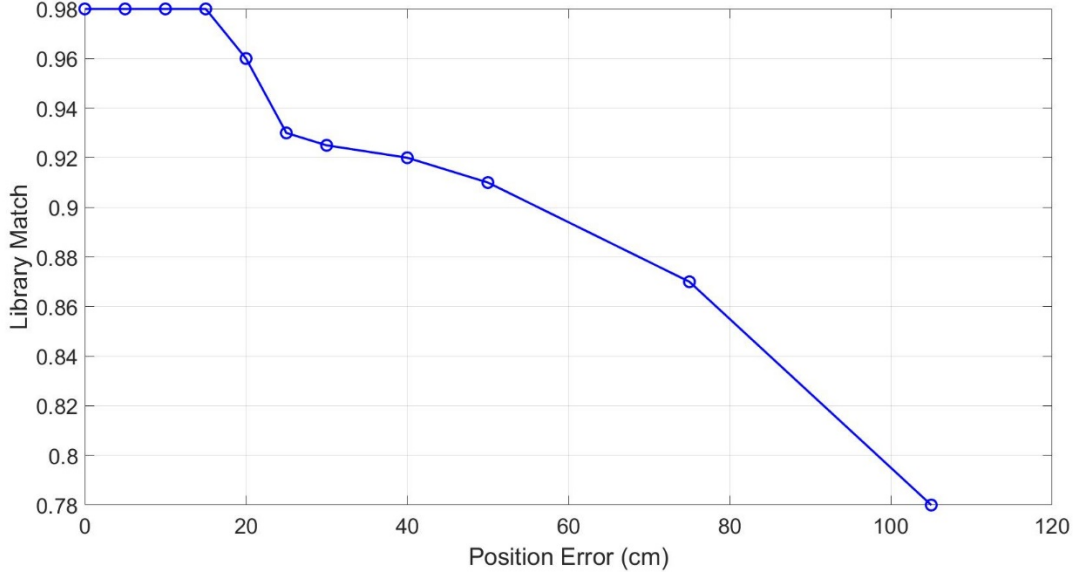


Figure 33. Library Match as a Function of Added Position Error.

These results indicate no decrease in classification quality for position errors of up to 15cm.

The library match maintained a consistent value of .98 for position errors of up to 15cm. Errors greater than 15cm resulted in a decrease in the library match; however, values above 0.9 were maintained for errors as great as 50cm. Errors greater than 50cm resulted in a significant decrease in classification performance. These results indicate that position errors for the sample-to-sample sensor displacement at the anticipated tow speeds should not have a significant impact on classification quality.

5.4 OBJECTIVE: EFFECTIVE PROCESSING METHODS FOR THE UNDERWATER ENVIRONMENT

Our dynamic processing flow includes a background correction step that applies a detrend filter to remove background responses that vary slowly with respect to the anomaly response. This approach works effectively for land surveys; however, to be effective in the underwater environment, the electromagnetic interaction between the seawater environment and the target during the receiver period must be negligible. In other words, the background removal process assumes:

$$\mathbf{R}_T^{air}(t_n) \approx \mathbf{R}_T^{sea}(t_n) - \mathbf{R}_B^{sea}(t_n) \quad 0.5 \text{ ms} < t_n < 10 \text{ ms} \quad (5.1)$$

Here \mathbf{R}_T^{air} is the response of the target in air, \mathbf{R}_B^{sea} is the background response of the seawater and seafloor, and \mathbf{R}_T^{sea} is the response of the target embedded in the seawater/seafloor environment.

To verify this assumption, we performed an electromagnetic modeling analysis using COMSOL Multiphysics and analytical models. Because we were interested in investigating the basic principles of background removal in the context of the underwater towed array, we simplified the sensor model for computational efficiency. The model used for this analysis included a co-axial, co-planar transmitter and receiver pair (both vertical dipole loops) placed above a steel sphere embedded in the seafloor. Figure 34 shows a representation of the model parameters.

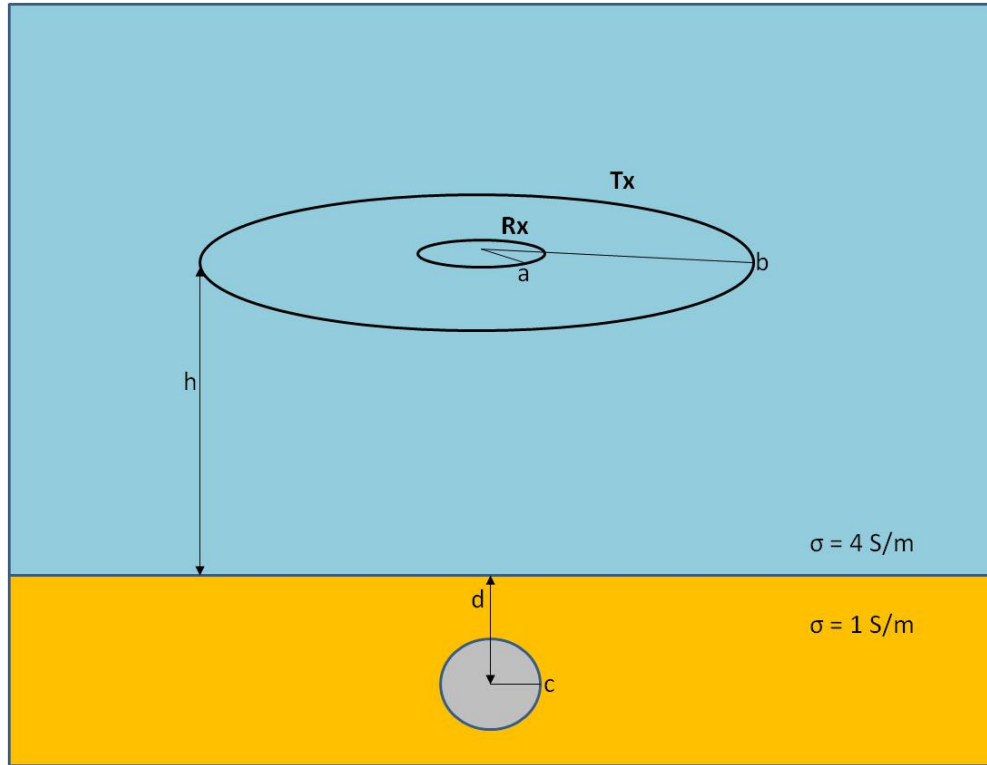


Figure 34. This Figure Describes the Basic Model Parameters.

a, b are the Rx, Tx loop radii; h is the sensor height above the seafloor; d is the depth of the steel sphere, c is the radius of the steel sphere. Assumed conductivities are 4 S/m and 1 S/m for the water and seabed, respectively.

We evaluated the effects of varying the different model parameters to understand whether the assumption in Equation 5.1 is valid for the expected operating ranges. Specifically, we modeled the effects of transmitter loop size, sensor standoff above the seafloor, and target depth below the seafloor.

5.4.1 Transmitter Loop Size

This case evaluates the effect of the transmitter loop size on background removal. For each loop size in Table 6, we evaluated the sphere response in air, the sphere response in the seawater environment, and the background response of the seawater environment. We then compared the sphere in-air response to the sphere in-water with the background response subtracted (Equation 5.1).

Table 6. Case 1: Transmitter Loop Parameters

RX radius a [m]	0.05
Standoff h [m]	2.0
Depth of Sphere d [m]	0
Diameter of Sphere c [m]	0.125
<i>Variables:</i>	
TX radius b [m]	0.5, 1.0, 1.5, 2.0, 2.5

Figure 35 shows the model results. For each simulation, we applied an axial-symmetric (2.5D) Finite-Element-Model using COMSOL Multiphysics 4.3a to determine the background and sphere response. For the background response, we also applied an analytical solution to determine the vertical magnetic field component and voltage induced in a coil embedded in a half space. Solutions for the vertical field are given by Edwards et al., 1987 and solutions for the induced voltage are given by Swidinsky et al., 2016. The analytical solutions provided confirmation of the numerical implementation.

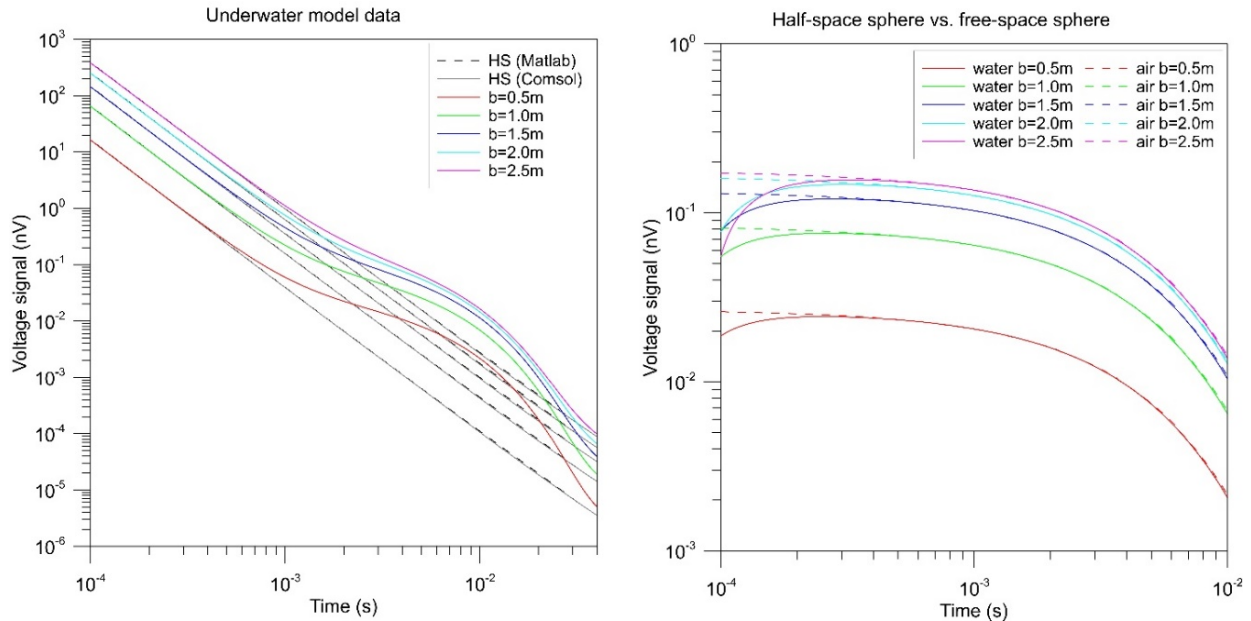


Figure 35. Sphere Response for Various Loop Sizes.

*LEFT: model data for the background (dashed: calculated in Matlab, solid: calculated in COMSOL).
 RIGHT: Comparison of the sphere solutions after subtraction of the (water/sediment) background model (solid lines) and the reference, where the sphere is located in free-space (dashed).*

The results demonstrate significant deviation from the in-air (free-space) response of the sphere compared to the background subtracted response, but only in the very early time (i.e., <200-500 microseconds). Even for the largest transmitter loop size (5-meter diameter), the background subtracted results match those of the in-air response for time gates later than approximately 500 microseconds.

5.4.2 Standoff

For the next test case, we adjusted the standoff height of the sensor coils above the seafloor to determine if this range had any effect on the background correction. Standoff parameters are listed in Table 7 and the model results for this test case are shown in Figure 36.

Table 7. Case 2: Standoff Parameters

RX radius a [m]	0.05
TX radius b [m]	1.5
Depth of Sphere d [m]	0
Diameter of Sphere c [m]	0.125
<i>Variables:</i>	
Standoff h [m]	0.5, 1.0, 1.5, 2.0, 2.5, 3.0

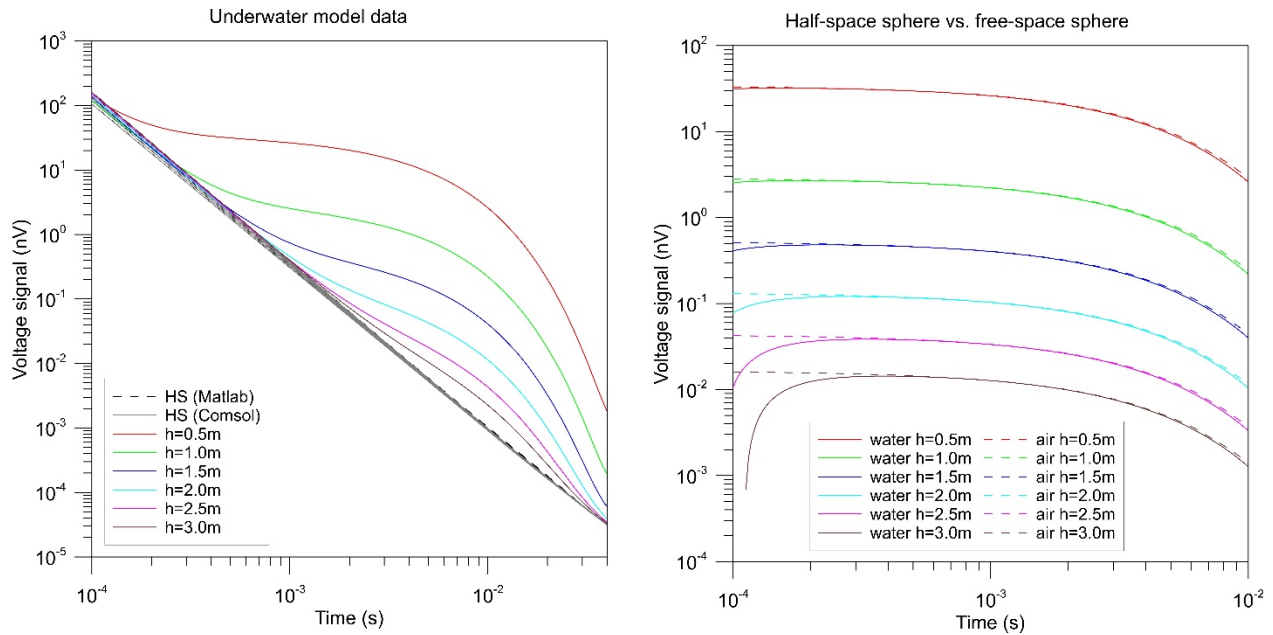


Figure 36. Sphere Response for Various Standoff Heights.

LEFT: model data for the background (dashed: calculated in Matlab, solid: calculated in COMSOL). RIGHT: Comparison of the sphere solutions after subtraction of the (water/sediment) background model (solid lines) and the reference, where the sphere is located in free-space (dashed).

Again, significant discrepancies between the in-air and background subtracted responses occur in the early time gates; however, these differences appear insignificant after approximately 200-300 microseconds.

5.4.3 Depth

For the final test case, we varied the depth of the target below the seafloor. These parameters are listed in Table 8 with model results shown in Figure 37.

Table 8. Case 3: Depth Parameters

RX radius a [m]	0.05
TX radius b [m]	1.5
Standoff h [m]	1.0
Diameter of Sphere c [m]	0.125
<i>Variables:</i>	
Depth of Sphere d [m]	0.25, 0.50, 0.75

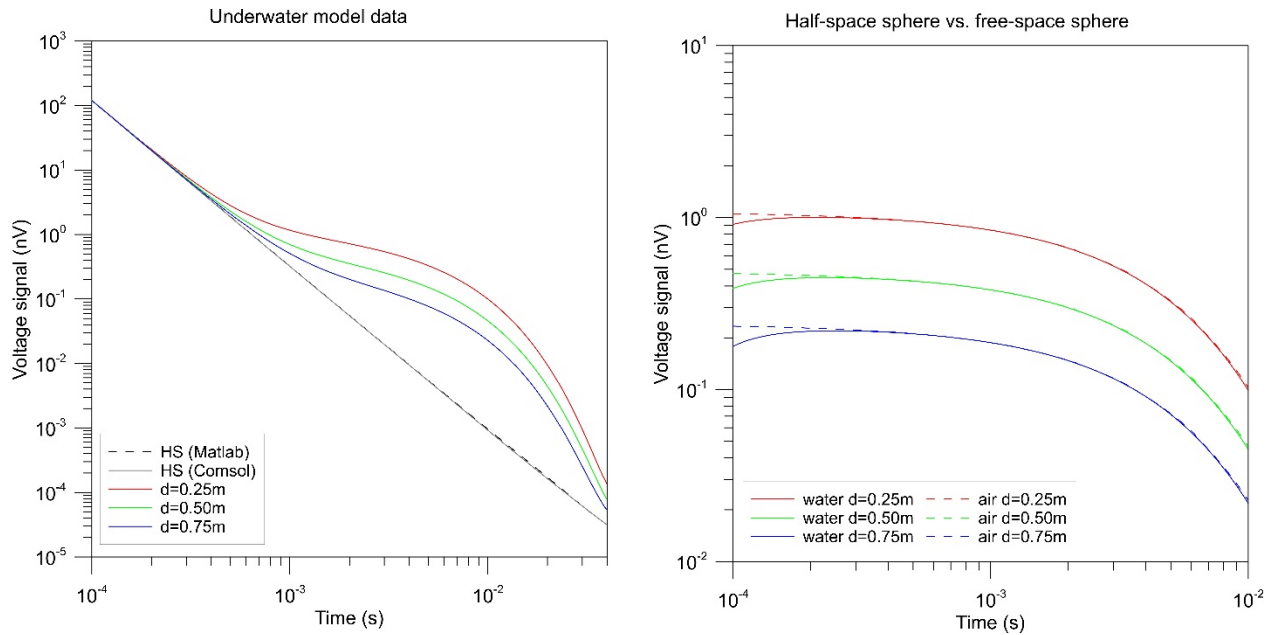


Figure 37. Sphere Response for Various Depths of the Sphere Below Seafloor.

LEFT: model data for the background (dashed: calculated in Matlab, solid: calculated in COMSOL). RIGHT: Comparison of the sphere solutions after subtraction of the (water/sediment) background model (solid lines) and the reference, where the sphere is located at the same distance in free-space (dashed).

This test case also demonstrated significant difference between the in-air and background subtracted responses in the early time gates, but no significant differences after 300-400 microseconds.

5.4.4 Sea Surface

At typical operating depths (e.g., >5 m), we anticipate that the sensor will be closer to the seafloor than it would be to the sea surface; however, to evaluate possible effects of the sea surface interaction, we evaluated the sea surface response to the transmitter field at frequencies corresponding to the early time (i.e., <1 ms). Figure 38 compares the sea surface response with the seafloor response at 1 kHz and 10 kHz frequencies. This frequency band corresponds approximately to the early decay period between 0.1 – 1 ms.

This model uses a transmitter loop embedded in a conductive half-space medium (seawater $\sigma = 4$ S/m) and calculates the in-phase and quadrature-phase components of the secondary field generated by the environment. For this application, we have set the conductivity of the second medium to either 0 or 1 S/m to simulate air and seafloor boundaries, respectively. The loop standoff from the boundary is varied to produce a response curve.

The response curves show that the sea surface and seafloor responses exhibit the same phase behavior, with the sea surface response amplitude slightly greater. Therefore, we expect that the background subtraction principles applied to seawater and sediment interactions would also be valid for sea surface interactions. At typical operating depths where the sensor is closer to the seafloor than the sea surface, the surface response will be significantly lower than the seafloor response. The most notable consideration may be the effects of surface variability when operating in shallow water. Significant surface waves (e.g., Sea State 3) while the sensor is at depths less than 3 meters would most likely cause variability in the background response, particularly in the early time gates (<1 ms). The frequency of this background variability would be a function of the wave frequency, the tow speed, and the tow direction with respect to the wave direction.

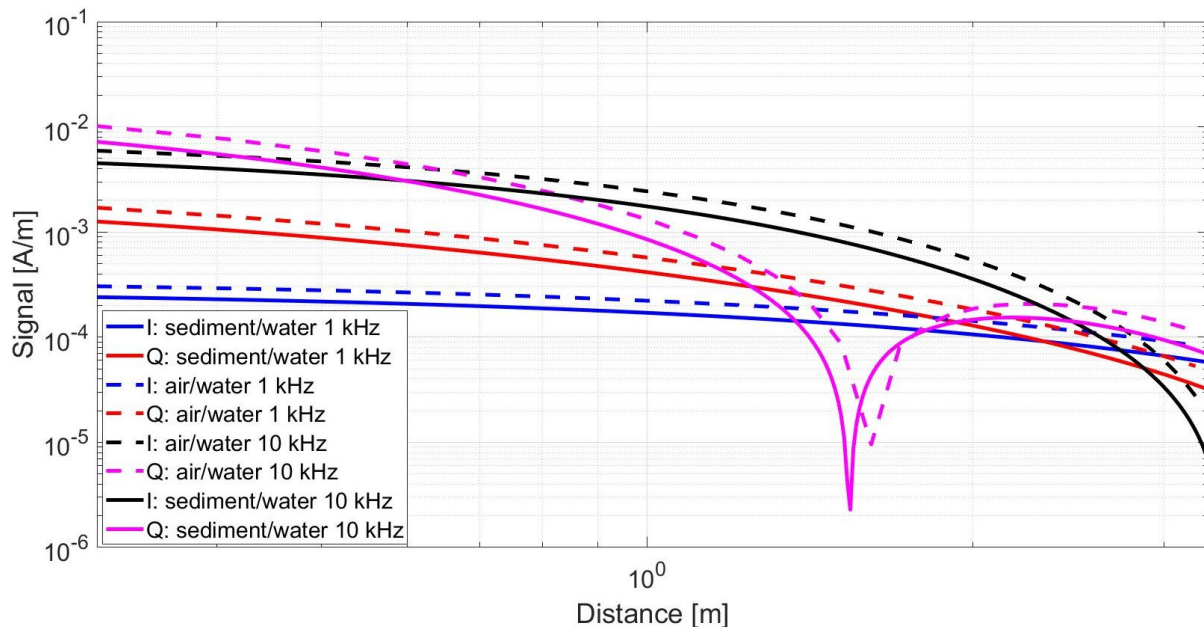


Figure 38. In-phase (I) and Quadrature-phase (Q) Response at 1 kHz and 10 kHz Corresponding to the Seafloor and Sea Surface Interaction with the Transmitter Field at Various Sensor Depths.

5.4.5 Conclusion

Our modeling indicates that there may be significant interactions between the seawater environment that would not be accurately accounted for using a simple background subtraction method. While these interactions may affect classification in the very early time, we do not anticipate that they will affect background subtraction methods in the 0.5 ms – 10 ms period that is more critical for classification. Therefore, we believe the standard background detrend methods used for land-based surveys should apply to underwater dynamic processing as well.

5.5 OBJECTIVE: ORIENTATION STABILITY

Our simulations in the ProteusDS environment started with stability load cases. We analyzed the roll and pitch response to initial displacements to determine array stability with respect to the seafloor.

5.5.1 Roll Response

If the towed EMI sensor rolls too much, it will be in danger of contacting the seabed due to the width of the sensor and the proximity of the sensor to the seabed (i.e. 1-2m altitude during operations). To increase the roll stability, either the distance between the center of gravity (CG) and center of buoyancy (CB) or the buoyancy force must be increased to increase the righting moment.

For the towed EMI sensor, it is difficult to increase the distance between the CG and CB by redistributing the locations of transmitter and receiver components, as the component locations are fixed due to the sensing requirements; however, we adjusted the buoyancy of the sensor array by adding buoyant flat plate surfaces at the top and sides of the sensor. These changes increased the roll stability significantly.

Load case S-01 in Table 5 tested the roll response of the towed EMI sensor under an initial set of static conditions. In this case, the towed EMI sensor was submerged with no tow speed. The bridles, clump, and towline were removed. The towed EMI sensor was placed at a roll angle of 30 degrees and was constrained in translation in the x , y , and z directions (coordinate frame depicted in Figure 15). The array was also constrained in rotation in the pitch and yaw direction, meaning the towed EMI sensor could only rotate about its center of gravity position in the roll (x) axis.

The roll response, shown in Figure 39, is slightly underdamped, but with minimal overshoot. Once a critical roll velocity is reached, the righting moment balances against hydrodynamic drag forces created by the rolling motion. The lower damping at low angular velocity results in slowly decaying roll about the neutral position. The system reaches +/- 5 degrees of the neutral orientation within 2.8 seconds.

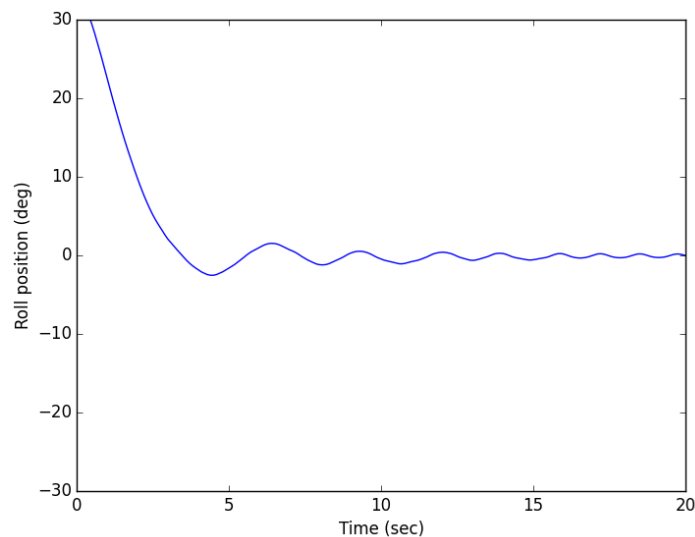


Figure 39. Load Case S-01, Roll Response of the Towed EMI Sensor.

5.5.2 Pitch Response

Load case S-02 tested the pitch response of the towed EMI sensor. For this case, the array was, again, submerged with no tow speed. The bridles, clump, and towline were removed from the system. The sensor was placed at a pitch angle of 30 degrees and was constrained in translation in the x , y , and z direction. The system was also constrained in rotation in the roll and yaw direction, meaning it could only rotate about its center of gravity in the pitch (y) axis.

The pitch response is shown in Figure 40. The towed EMI sensor in this configuration produces an underdamped response in pitch. The pitch DOF has less hydrodynamic damping than the roll DOF, as the drag forces have shorter moment arms about the pitch axis. Additionally, the moment of inertia about pitch is much smaller and thus the response is faster.

The sensor requires about 20 seconds to reduce oscillations such that it remains within ± 5 degrees of the neutral pitch position. The neutral pitch position in no current (i.e. no forward tow speed) is 0 degrees. This zero-pitch angle indicates that the center of buoyancy is directly above of the center of gravity.

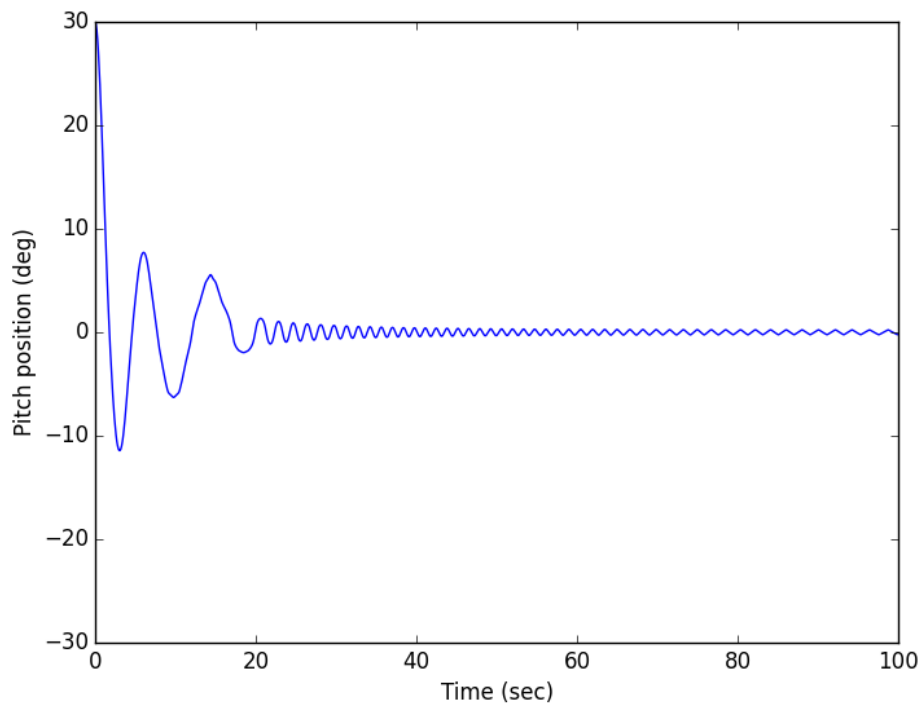


Figure 40. Load Case S-02, Pitch Response of the Towed EMI Sensor.

5.5.3 Conclusion

In both the roll and pitch cases, the sensor array is somewhat underdamped; however, it settles relatively quickly (~ 3 seconds for roll and ~ 20 seconds for pitch) to within ± 5 degrees after a large perturbation of 30 degrees. During operation, it is unlikely that the sensor would frequently encounter such large disturbances. For example, changes in pitch angle would more commonly be associated with altitude adjustments, which would produce significantly smaller angles.

5.6 OBJECTIVE: POSITION STABILITY

After assessing the righting moment cases (S-01 and S-02), we evaluated array stability under dynamic loads. This analysis required calculation of the drag forces encountered during towed operation. To evaluate cases where hydrodynamic shielding would reduce drag, we performed drag analysis using the computational fluid dynamics (CFD) package Virtual Wind Tunnel (VWT) by Altair. The analysis provided the total drag loading on the sensor in 1.5 m/s flow (3 knots) for the pitch angles of 0, 45, and 90 degrees. This analysis accounted for all hydrodynamic shielding acting on the surfaces.

We determined that sensor pitch would cause significant shielding as the bottom plate (with the receivers and receiver plate) obstructed the rest of the sensor. Thus, the structure was pitched in VWT to determine this effect. Drag force change as a function of yaw is highly dependent on the side plate drag, which is calculated in ProteusDS using flat plate lift and drag tables. Significant shielding would not occur due to sensor yaw; thus, no yaw orientation was analyzed in VWT. The model setup in the VWT software is shown in Figure 41. The resulting streamlines and surface pressures are shown in Figure 42 and Figure 43.

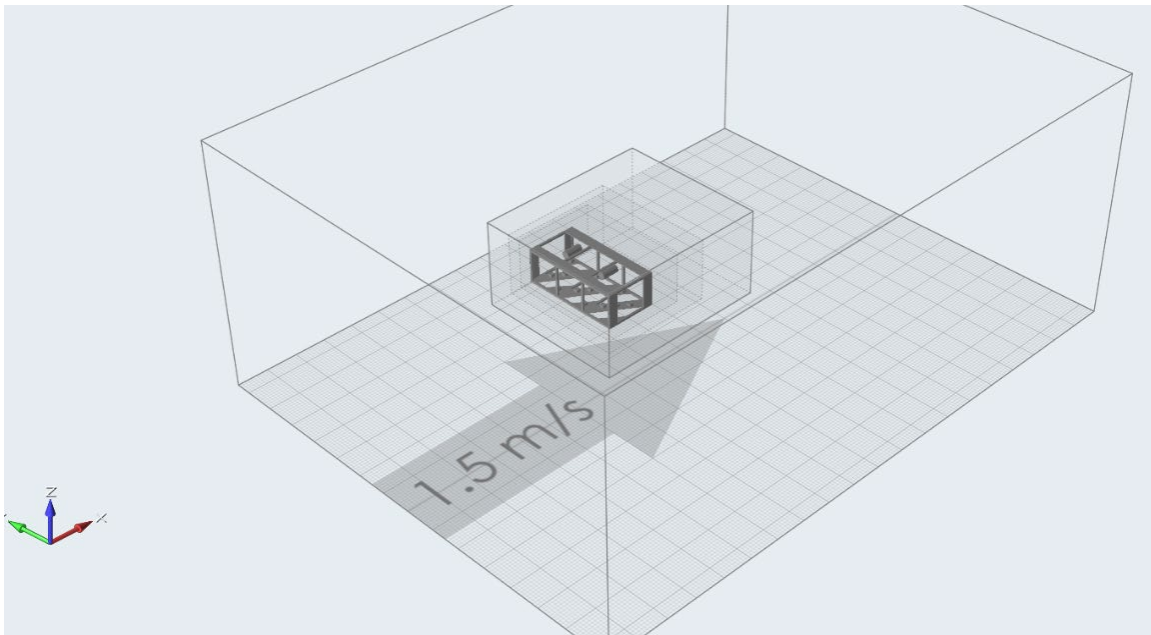


Figure 41. Setup of Towed Sensor Array in Virtual Wind Tunnel, with Refinement Zones Shown.

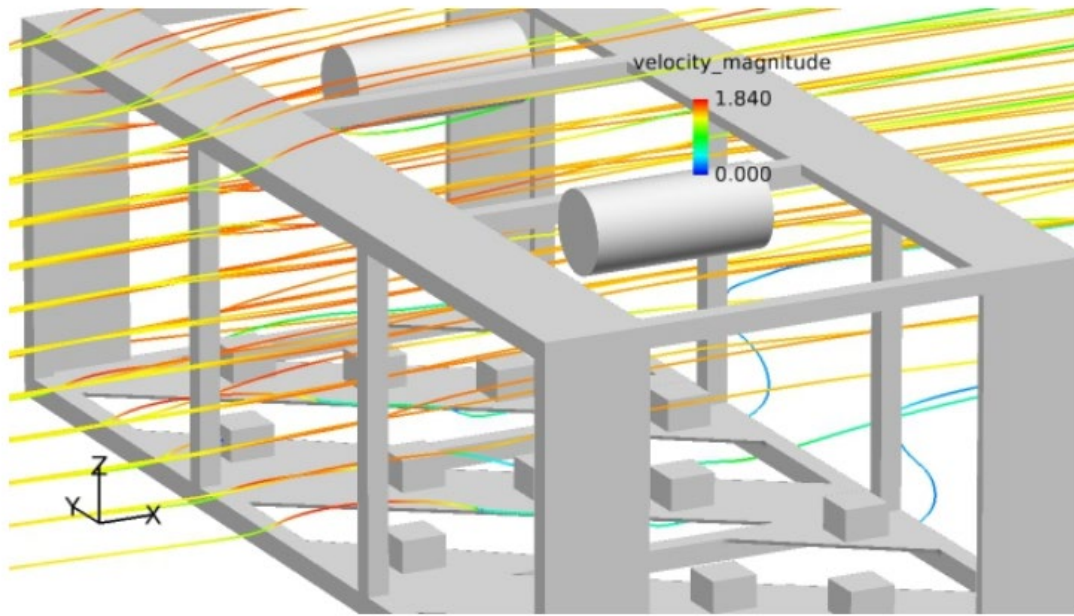


Figure 42. Streamlines of Towed Sensor Generated in Virtual Wind Tunnel.

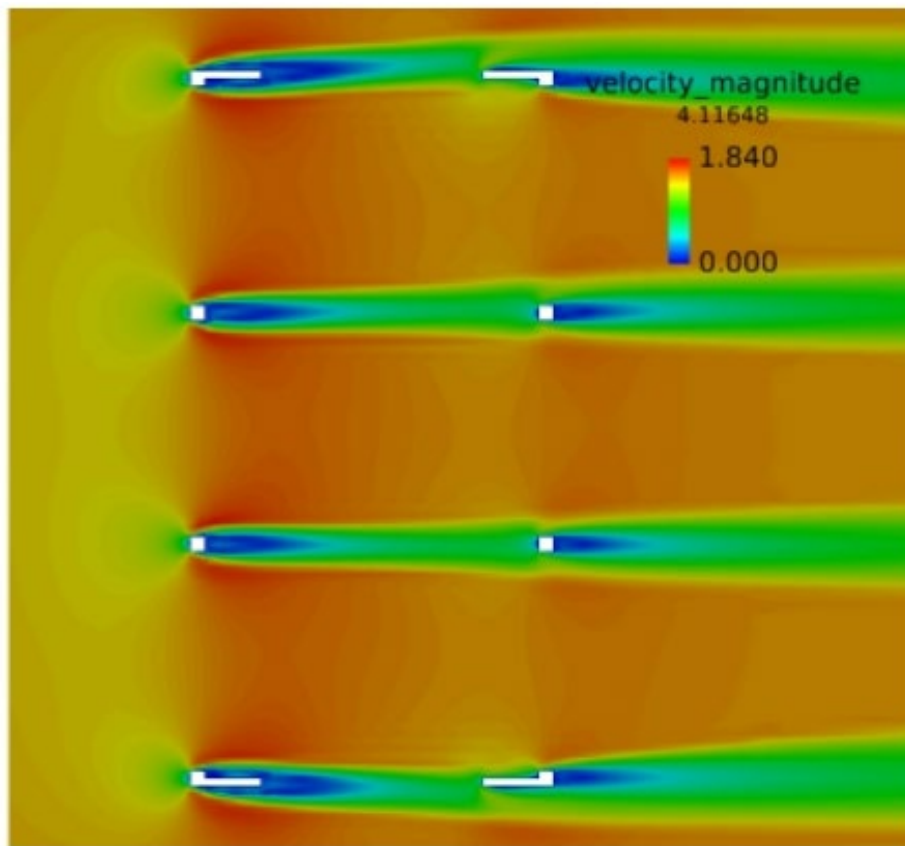


Figure 43. Velocity Magnitude Demonstrating the Shielding Effect Captured in Virtual Wind Tunnel

VWT provides the drag area of the structure, where drag area is the drag coefficient multiplied by the frontal area for the entire structure:

$$F_d = 0.5 * \rho * A * C_d * u^2 \quad 5.2$$

$$drag\ area = A * C_d$$

Where:

F_d is the drag force.

ρ is the fluid density, 1025 kg/m³ used for seawater.

A is the frontal area.

C_d is the drag coefficient.

u is the relative fluid velocity.

An explicit frontal area calculation is not performed in VWT; thus, the drag area value is used. ProteusDS calculates frontal area by using the front faces of all the hydrodynamic meshes. To ensure the drag force calculations in ProteusDS are accurate, the drag area from VWT is divided by the frontal area of the structure in ProteusDS to yield a drag coefficient to be used in ProteusDS. The ProteusDS frontal area was calculated by summing all the mesh faces in the ProteusDS model in the surge direction. The drag area results from VWT, the frontal area calculations, and the resulting required drag coefficient are shown in Table 9. The drag on the towed EMI sensor in the surge direction for varying flow speeds is shown in Figure 44.

Table 9. Drag Area Results from VWT, drag Coefficients Required in ProteusDS.

Pitch angle (deg):	VWT Drag area (m ²):	ProteusDS frontal area (m ²):	ProteusDS Surge direction drag coefficient:
0	1.439	1.640	0.87
45	4.732	Not calculated	N/A
90	5.242	6.113	0.85

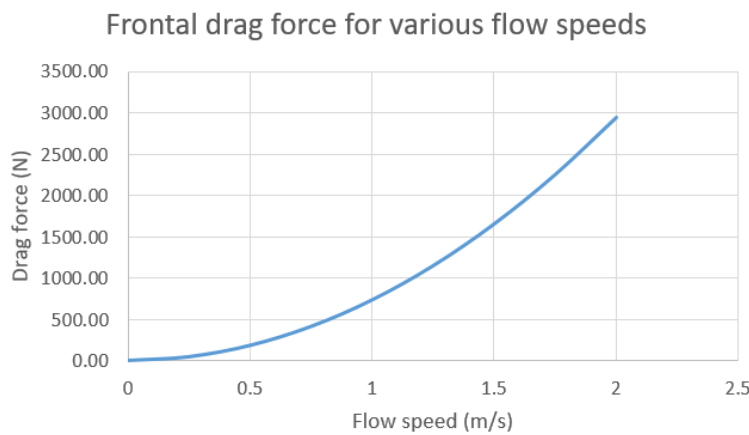


Figure 44. Drag Force as a Function of Flow Speed for the Towed Array Sensor with a Pitch Angle of 0 Degrees.

The drag loads in the sway direction are dominated by the vertical flat plates. These plates are represented in ProteusDS using a foil model that samples the relative fluid velocity and angle of attack of the foil and applies lift and drag forces accordingly. The lift and drag coefficients for each angle of attack are provided for a flat plate from literature (Blevins, 1984). The flat plate has a drag coefficient of 1.05 at an angle of attack of 90 degrees (perpendicular to flow). Due to the width of the towed EMI sensor, minimal shielding will occur during towing.

The frontal area in the sway direction, excluding the flat plates, is 1.52m^2 . The drag coefficient on all surfaces, excluding the flat plates is 0.85. The frontal area in the sway direction of the flat plates is 1.284m^2 . The flat plate drag coefficient is 1.05.

The heave drag coefficients were determined from the VWT analysis with a pitch angle of 90 degrees. The frontal area in the heave direction is 6.113m^2 . The drag coefficient used in ProteusDS for the heave direction was 0.85.

5.6.1 Sway Response

Load case S-03 tested the sway response of the towed system. In this case, the sensor was laterally offset 10m in the global Y direction from the neutral position (the tow point moves along the global X direction). This scenario required the towed EMI sensor to re-align with the tow point (i.e. where the global $Y=0\text{m}$) at a tow speed of 1.5m/s. Layback was calculated assuming a water depth of 30 meters.

The sway response is shown in Figure 45. The righting force, which causes the sensor to align with the flow at a neutral position, is caused by the lateral drag forces acting on the sensor surfaces that are not aligned with the flow. As the sensor nears the neutral lateral position, the sensor yaw angle is reduced and there are fewer surfaces exposed to the flow, reducing the amount of lateral drag force. Therefore, as the towed EMI sensor nears the neutral position, the sway velocity decreases. The system is within 0.5m of the final position after 500 seconds. No overshoot occurs.

The response of the towed EMI sensor in sway has low priority when compared with the response in other degrees of freedom. It was assumed that situations that result in a requirement for faster sway response are unlikely to occur. Additionally, sway response speed can only be easily improved by increasing frontal drag on the towed EMI sensor, which would require longer layback and heavier clump weights.

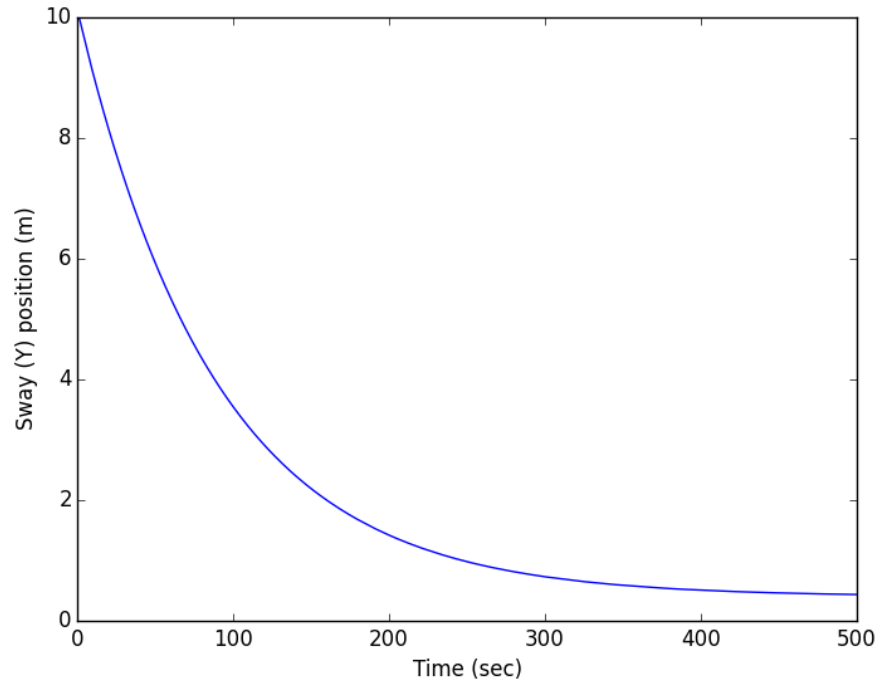


Figure 45. Load Case S-03, Sway Response of the Towed EMI Sensor with 1.5 m/s Tow Speed.

5.6.2 Heave Response

Load cases S-04 and S-05 tested the heave response of the towing system. The towed EMI sensor was offset 10m in the global Z direction from the neutral position. In case S-04, the towed EMI sensor was located 10m above the neutral position and, therefore, needed to descend in the water column to reach the neutral configuration. In case S-05, the sensor was located 10m below the neutral position and, therefore, needed to rise in the water column to reach the neutral configuration. The seabed was removed from the simulation for these test cases to ensure that no seabed contact occurred. A tow speed of 1.5 m/s was used.

The heave responses for both cases are shown in Figure 46. The response in heave is very similar for both the rising and falling case. The system reaches the final position in 160 seconds for case S-04 and 150 seconds for case S-05. No overshoot occurs.

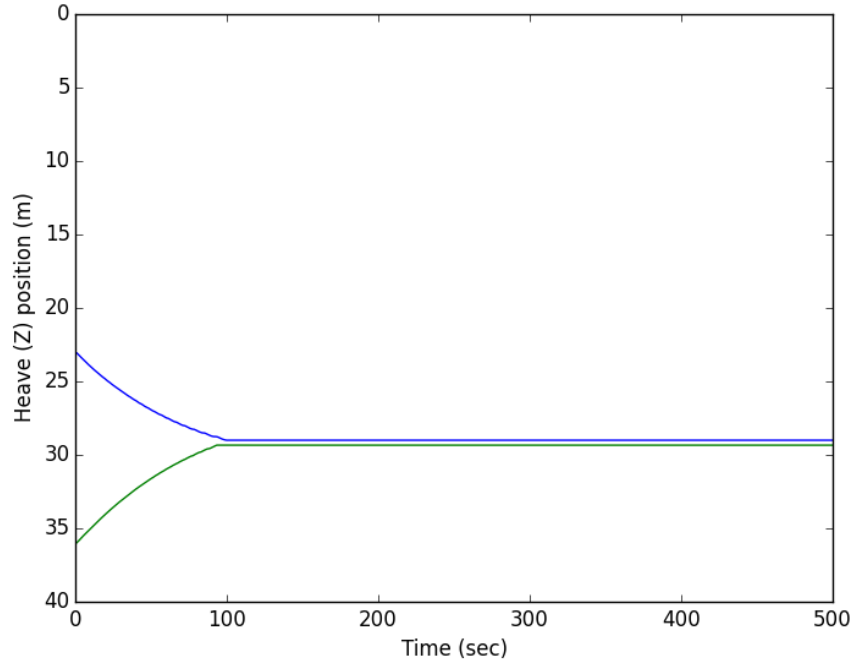


Figure 46. Load Case S-04 (Blue) and S-05 (Green), Heave Response of the Towed EMI Sensor (Rising and Falling) with 1.5 m/s Tow Speed.

5.6.3 Conclusion

For both heave and sway offsets, the towed array stabilizes to the neutral position; however, this response requires significant time, particularly for the sway offset, which requires approximately 500 seconds to obtain a position within 0.5m of neutral. This effect would be most significant for turning operations. Therefore, this delayed response should be accounted for in the survey design, most likely by pay-in of the line before turning. It should be emphasized that the settle time can be reduced by increasing drag surface; however, this adjustment would require increased layback and clump weight as well.

5.7 OBJECTIVE: STANDOFF STABILITY

To understand the effects of seafloor standoff variability due to surface motion, we simulated wave induced tow point heave and surge. Load cases S-06 and S-07 tested the response of the towed EMI sensor in the presence of waves. The waves represented Sea State 3 with a wave height of 1.25m and a period of 5 seconds. Uniform (Airy) waves were used for this simulation. Load case S-06 featured head seas (waves into the bow of the tow vessel) and an encounter frequency of 1.45 rad/sec while load case S-07 featured following seas (waves into the stern of the tow vessel) and an encounter frequency of 1.06 rad/sec.

The heave response of the towed EMI sensor is shown in Figure 47. The heave response is relatively small compared to the tow point heave, with peak to trough oscillations of 0.3 m occurring for both cases. Both cases also exhibit a rising of the towed EMI sensor of 1.5m in the Z direction. The rising of the towed EMI sensor is due to the inertia of the clump weight. The wave period causes the clump to rise faster than it descends, resulting in a higher neutral tow position.

The difference in encounter frequency has no notable effect on the system. The heave positions of the tow point for the different encounter frequencies are shown in Figure 48. Peak and mean tensions on the towline are shown in Table 10.

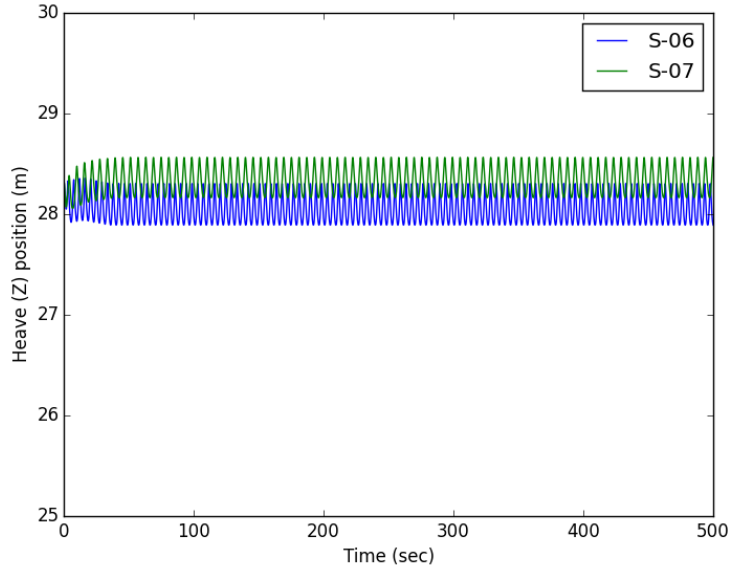


Figure 47. Load Case S-06 and S-07, Heave Position of the Towed EMI Sensor in Waves (Head and Following) with a 1.5m/s Tow Speed.

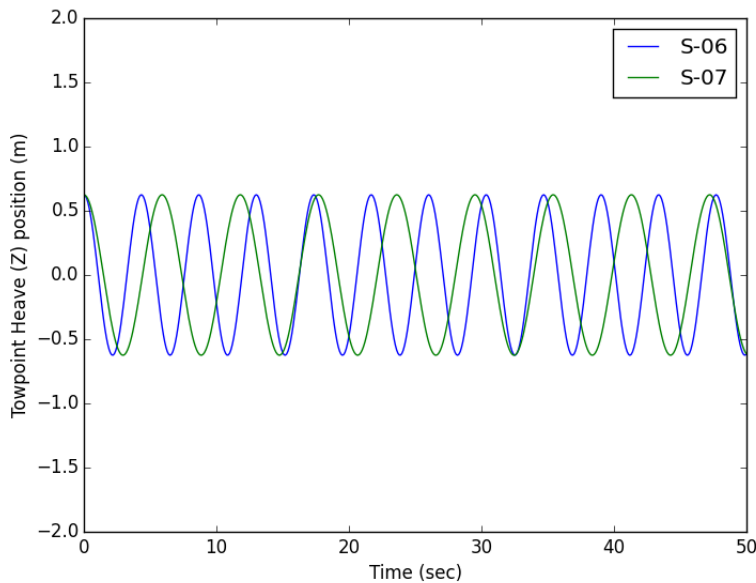


Figure 48. Load Case S-06 and S-07 Tow Point Heave Position.

The encounter frequency of the waves is different for head waves and following waves.

Table 10. Towline Tensions for Load Case S-06 and S-07.

Load case:	Mean tension - Bottom (kN):	Max tension – Bottom (kN):	Mean tension - Top (kN):	Max tension - Top (kN):
S-06	2.32	4.98	2.44	5.20
S-07	2.26	4.09	2.37	4.28

In practice, the +/-15 cm heave encountered by the towed array represents a worst-case scenario since the surface vessel will likely provide some damping at the tow point. This scenario also assumes the most difficult operating conditions expected for the towed survey. Therefore, we do not anticipate that surface induced standoff variability will be problematic for towed array operation. The main consideration is the change in mean standoff, which would need to be compensated for by the towline pay-out.

5.8 OBJECTIVE: DEPTH CONTROL RESPONSIVENESS

To assess the responsiveness of the control system to changes in depth, we performed a series of controlled load simulations applying a constant winch pay-in speed. Cases C-01 to C-09 tested the response of the towed EMI sensor to changes in towline length based on winch speed. The seabed was removed from the simulation for these load cases to ensure that no seabed contact occurred. The tow speed and clump weight mass were changed for each case to determine the effect of these variables on the altitude (i.e., heave position and velocity) of the towed EMI sensor when using the winch.

Tow speeds of 1.0 m/s, 1.5 m/s, and 2.0m/s and clump weights of 25kg, 50kg, and 75kg were tested as variables. A constant winch speed of 0.22 m/s was used based on towline tension values from earlier simulations and a relevant winch specification (see e.g., <https://www.warn.com/truck/winches/M8274-50.jsp>). The tow speed and clump weight and corresponding heave velocity of the towed EMI sensor when winching the towline are shown in Table 11.

Table 11. Tow Speed, Clump Weight, and Vertical Velocity of Control Load Cases.

Test number:	Tow speed (m/s):	Clump weight (kg):	Vertical (heave) velocity (m/s):
C-01	1.0	25	4.3x10 ⁻²
C-02	1.0	50	7.1x10 ⁻²
C-03	1.0	75	9.6x10 ⁻²
C-04	1.5	25	3.2x10 ⁻²
C-05	1.5	50	4.3x10 ⁻²
C-06	1.5	75	5.4x10 ⁻²
C-07	2.0	25	2.2x10 ⁻²
C-08	2.0	50	3.2x10 ⁻²
C-09	2.0	75	4.2x10 ⁻²

The vertical velocity of the towed sensor is purely a function of the winch speed and towline angle shown in Figure 17. Increasing the clump weight and reducing the tow speed result in higher heave velocities (i.e. faster changes in altitude) of the towed EMI sensor when winching. Faster tow speeds increase the hydrodynamic drag on the platform and increase the layback of the system, thereby decreasing the towline angle and vertical velocity. Larger clump weights decrease the layback of the system, thereby increasing towline angle and vertical velocity. The fastest vertical velocity is 9.6×10^{-2} m/s at a tow speed of 1.0 m/s with a clump weight of 75kg. The slowest vertical velocity is 2.2×10^{-2} m/s at a tow speed of 2.0 m/s with a clump weight of 25kg.

For some perspective, a 10 cm/s vertical change at 1.0 m/s tow speed means the system could respond to a constant 10% incline of the seafloor. Thus, it should be possible to respond to changes in seafloor incline/decline; however, operating speed and corresponding towline angle, as well as clump weight are important considerations in the survey design. For example, a heavier clump weight may be required to operate in areas where more significant inclines/declines will be encountered.

5.9 OBJECTIVE: OPERATING LOAD FEASIBILITY

Cases O-01 to O-04 evaluated the steady-state towline loads encountered at different operating speeds to ensure that these remain well within operating specifications of the equipment. The towline length was set to ensure that the towed EMI sensor maintained a depth of 29m. The layback and towline tensions for each case are shown in Table 12.

Table 12. Layback and Towline Tensions for Load Cases O-01 to O-04.

Case:	Tow speed (m/s):	Layback (m):	Towline tension - Bottom (kN):	Towline tension - Top (kN):
O-01	0.5	23.8	0.27	0.56
O-02	1.0	78.5	1.10	0.98
O-03	1.5	143.5	2.24	2.28
O-04	2.0	273.6	3.87	4.02

We also evaluated maximum towline tension during startup. Case O-07 starts from a 30m resting clump weight depth (the EMI sensor is above the clump weight due to its net buoyancy of 5kg). The tow speed is instantly increased to 1.5m/s and the clump is lifted off the seabed and the towed EMI sensor responds. Towline loads during startup are shown in Table 13.

Table 13. Towline Tensions During Start Case O-07.

Max towline tension - Bottom (kN):	2.99
Max towline tension - Top (kN):	3.13

We selected the properties of a 14mm Amsteel Blue rope for the towline. This line size was chosen to ensure enough strength for a power and data cable of similar size. The minimum breaking strength of 14mm Amsteel Blue is 16,500 kg. Thus, for the greatest tension encountered (O-04), this strength results in a factor of safety of 40.

5.10 EFFECTIVE TARGET LOCATION TRACKING

Target location tracking accuracy is a function of the combined sensor array position and target localization errors. Sensor array position will be estimated using forward kinematics from the tow point on the surface vessel. Target localization is based on the position estimates obtained from inversion of the dynamic data.

Kinematic transformation of the towline azimuth, line length, and sensor depth provide an estimate of the horizontal position (layback) of the sensor. Towline azimuth and winch pay-out (line length) are measured at the tow point on the surface vessel. Sensor depth is determined from the difference between the tow vessel and the sensor altimeters. The primary source of error will be from this depth measurement. For a fixed amount of depth measurement error, the layback position error varies only slightly with the actual sensor depth. Figure 49 shows layback error as a function of depth measurement error at a tow speed of 1.5 m/s and operating depth of 30 meters.

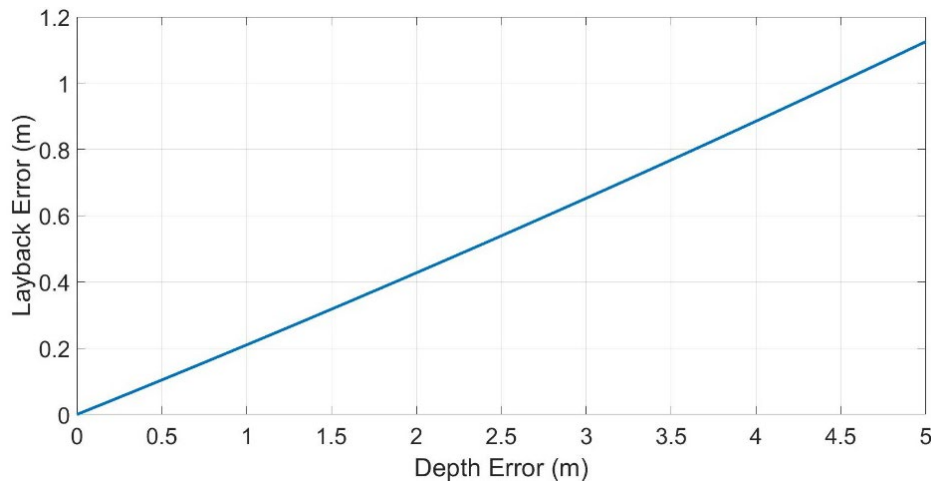


Figure 49. Layback Error as a Function of Depth Measurement Error at 30-meter Operating Depth.

Accurate measurement of the towline azimuth will be important for sensor position tracking in cross-currents. Our hydrodynamic analysis of operations in cross-currents (stability load cases S-08 and S-09 in Table 5) yielded a towline azimuth of 19 degrees at 0.5 m/s cross-current and an azimuth of 34 degrees at 1.0 m/s cross-current. Thus, cross-currents may result in significant lateral offset of the sensor array. Under such conditions, we estimate that encoder accuracy will need to be within 0.5 – 1.0 degree to maintain lateral position accuracy of 0.5m or better (encoder accuracy requirements are dependent on operating depth and tow speed, which determine the layback).

Additional sources of sensor position error include cable catenary, which will depend on the towline mass and buoyancy. These parameters will be specific to the cable selected for the towline. If the towline is close to neutrally buoyant, the catenary should have minimal effect. Adjustments to the line length measurement can be made to account for the catenary if the towline tension is also measured. This information can be applied to the catenary equation to provide the corrections.

Target localization is obtained from inversion of the dynamic data. We have demonstrated that the dynamic classification approach reliably provides target location estimates within 15 cm accuracy. Table 14 shows the mean localization error values and standard deviation obtained from dynamic OPTEMA data for all TOI encountered at the SWPG demonstration.

Table 14. Mean Location Error and Standard Deviation for TOI Location Estimates.

	RF-15 FOCUS AREA TOI		
	Mean Error (cm)	Standard Deviation (cm)	Maximum Error (cm)
Northing/Easting	5.5	2.4	11.8
Depth	3.3	4.6	14.0

Target localization accounts for variability in the orientation of the sensor by applying roll and pitch corrections to the inversion output. These roll and pitch measurements, usually recorded by an inertial measurement unit (IMU), are incorporated in the inversion model to transform relative target location estimates to absolute (e.g., global) position estimates. We anticipate using the same IMU that we implemented on the OPTEMA sensor for dynamic classification on land. This IMU is compact (44 mm x 24 mm x 11 mm) and can be mounted inside the electronics bottle, so will not affect sensor hydrodynamics. We have observed that proximity of the IMU to the transmitter coils may cause a shift in the heading output due to the magnetic field interference with the heading magnetometers; however, this is not an issue with dynamic classification sensors since the heading can be calculated from the GPS (and towline azimuth in this case).

Combining the target location and sensor position errors, we believe it will be possible to keep total target location error to less than 0.5m. The largest contributor to the total error will most likely be from the sensor position estimates obtained from the line length and depth calculations; however, for the expected towline angles, these position estimates appear tolerant of depth error (e.g., 2m depth error results in <0.5m layback error). Nonetheless, depth error may become more significant in difficult surface conditions or if seafloor variability is substantial.

6.0 COST ASSESSMENT

The cost benefit of applying dynamic classification underwater could be even greater than it is on land. While there is not yet substantial data to support cost benefit analyses of underwater classification, we can make some estimates of the potential cost benefit of this technology by extrapolating land survey cost data. We can start by considering the cost analysis in the recent Spencer Range Summary Report (ESTCP, 2014). This analysis estimates that cued classification surveys on land can provide about a 50% cost reduction over standard DGM and dig practices (i.e., no classification). This estimate assumes that it costs about \$125 to reacquire and dig each anomaly and that the cued classification survey can achieve about 80% clutter rejection. If we implement a dynamic classification survey that eliminates the need for a follow-on cued survey, we expect that it would be possible to get the same 50% cost reduction with only a 70% clutter rejection rate. This estimate assumes that the cost of the dynamic survey along with the cost of classification analysis is about 5x as expensive as the DGM survey and target pick analysis (\$5000/acre vs. \$1000/acre). This assumption is fairly conservative (the dynamic survey costs may in practice be closer to 2-3x the costs of standard DGM); however, this estimate gives a reference point for the expected cost breakdowns for the different surveys performed on land.

To understand how these costs would translate to underwater operations, we first need to consider the basic costs of target reacquisition required for remediation underwater. Based on past experience working with EOD dive teams, we estimate that it costs about \$1000/anomaly for diver reacquisition (\$20k/day for a dive team that can perform about 20 reacquisitions each day). We can assume that a standard DGM survey (i.e., magnetometer array or EM61s array) may be somewhat, but not significantly, more expensive to implement in water. While there are not significant cost data available for such surveys, we can reference relevant reports (see, e.g., AETC, 2005). In general, underwater DGM production rates should be comparable to those on land since the survey speeds are about the same. We can expect some increase in overall production cost since the field team may require more personnel and equipment rentals may be more expensive for underwater surveys; therefore, we apply a factor of 2x over land survey costs to achieve a baseline \$2000/acre for underwater DGM (survey plus data analysis). Since we anticipate a slightly lower production rate for underwater dynamic surveys (e.g., 3 knot tow speed for dynamic classification vs. 5 knots for DGM) and we need to include the cost of classification analysis as well, we will apply a fairly conservative gain of 5x over the DGM costs to estimate that underwater dynamic classification surveys would cost about \$10,000/acre (again this is probably a fairly conservative estimate).

Using these very rough estimates for underwater production and reacquisition costs, we now obtain the same 50% cost reduction using dynamic classification with just 50% clutter rejection needed. At this time, we have not considered underwater cued classification since currently it would be difficult to provide estimates of what cued underwater survey production costs might be (we can only assume they would be much higher than those on land). Thus, even with very basic cost assumptions it is apparent that an effective underwater dynamic classification system could enable significant cost savings even with fairly modest classification performance (i.e., 50% clutter rejection).

Page Intentionally Left Blank

7.0 CONSIDERATIONS FOR IMPLEMENTATION

We can summarize the results of our design study in terms of the main considerations for implementing classification (i.e., those related to achieving reliable classification performance underwater) and the considerations for operational feasibility (i.e., those related to the specific operation of the underwater towed system).

7.1 CONSIDERATIONS FOR UNDERWATER DYNAMIC CLASSIFICATION

Throughout the design study, we assessed requirements for adapting land-based dynamic classification methods to the underwater environment. Results from our analyses indicate that the basic principles of our classification approach will be transferrable to underwater operation. Our study demonstrated that the towed array configuration can provide reliable classification features at the targeted operational standoff. We assessed implementation of processing steps, such as background compensation, that will be critical for effective classification. Results indicate that the standard dynamic processing flow used on land should be applicable to underwater data, except for possibly the earliest time gates (i.e., <200-500 microseconds) where seawater interaction with the target may be significant.

Additionally, the single shot classification method we have used successfully for land surveys may be particularly beneficial for underwater surveys where degraded positioning quality will be a factor. This approach appears robust against sample to sample positioning error, which may be encountered during tow point surge. While cumulative errors over large tow distances may be relatively small for constant tow speeds, towline surge due to wave action may produce relatively large errors in sample to sample positioning.

The greatest risk for classification quality during implementation of this system is most likely due to the unknown noise characteristics of the dynamic underwater environment. From our study, we know that the characteristics of noise in the data have a significant impact on the reliability of classification features (i.e., whether the polarizabilities are well constrained). At this time, we do not have a substantial amount of data acquired dynamically in the underwater environment to determine, with certainty, the expected noise characteristics. During our study, we applied dynamic noise characteristics captured on land to create synthetic data. We believe this noise is relevant because it captures motion induced changes in receiver flux that should be encountered underwater as well; however, there may be additional noise features, particularly in the early time gates, that are not present in data acquired on land.

To mitigate this risk, we believe it will be possible to increase the effective transmitter power to improve SNR as needed for reliable classification. Our design demonstrates the uniform field characteristics at target depth that are required for high quality classification. If noise levels prove higher than anticipated, it may be possible to overcome these SNR limits with greater transmitter power. For example, the land-based OPTEMA system operates at an effective transmitter power of approximately 100 A-turns. For our simulations, we increased this level to 200 A-turns for the underwater system. This level is still fairly modest and could most likely be increased further if necessary to improve SNR. The primary limitation in the hardware design is to ensure that the transmitter components can handle the higher kickback voltages at greater power levels.

7.2 CONSIDERATIONS FOR TOWED OPERATION

Our hydrodynamic analysis included a comprehensive assessment of the key factors related to the operational performance of the system. The results indicate that the system design offers a hydrodynamically stable configuration that should meet the positioning and stability objectives for enabling effective classification. The 3D transmitter design provides a framework that enables vertical separation of the center of gravity and center of mass in a way that maximizes righting moment when a roll or pitch perturbation is encountered. Results from our simulations demonstrated that the system should enable operation in relative proximity to the seafloor (i.e., 1-2m standoff).

Specific design considerations related to operational feasibility of the system include:

1. Sway response of the system was notably slow for large sway offsets. This slow response is due to the lack of surface area exposed to the flow at small yaw angles. This effect may be most noticeable when turning. The system may require several minutes to obtain alignment with the tow point after large turns. This effect can be mitigated through pay-in of the towline during turns. Additionally, increased frontal drag area will improve the sway response; however, more drag results in greater layback and clump weight.
2. Tow point heave due to surface conditions should have a minimal impact on standoff variability (+/- 15cm in worst case operating conditions); however, our simulations indicated that it may cause a net offset in standoff. This offset can be compensated for with towline length adjustment.
3. Depth control responsiveness varies considerably with towline angle. Higher tow speeds (more drag) produce more layback and a lower towline angle, which reduces the vertical component of the winch pay-in velocity. Our simulations indicate that responsiveness to inclines of 10 degrees should be obtainable under typical survey conditions. For greater responsiveness to seafloor variability, lower speeds or larger clump weights should be applied.
4. Sensor position error will most likely be the greatest contributor to overall (global) target localization error. Accurate measurement of the sensor depth will be critical. Additionally, if cable catenary is significant, towline tension will need to be monitored to adjust for these line length offsets.

7.3 CONCLUSION

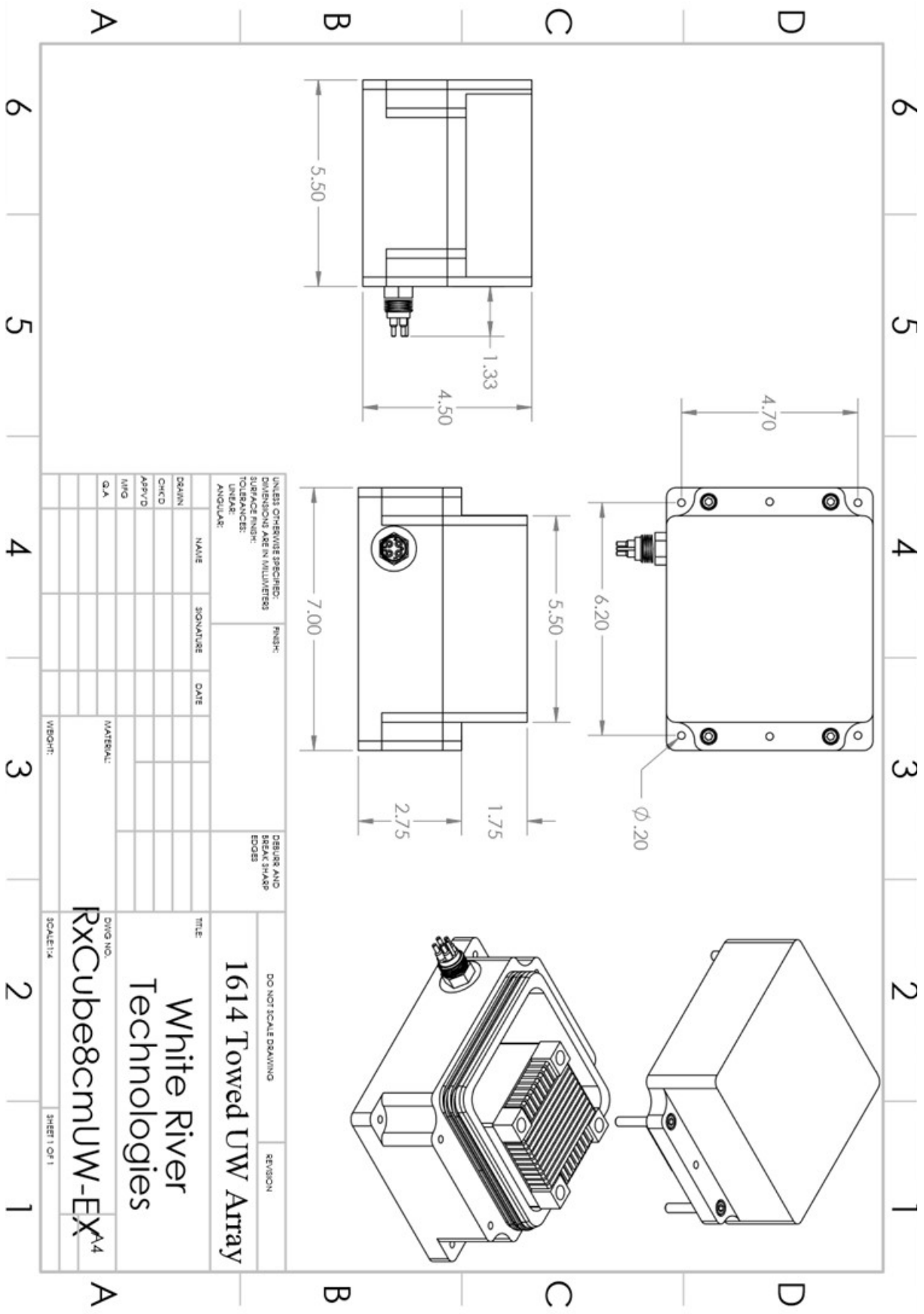
This concept feasibility study culminated with the design of an underwater dynamic classification sensor based on advanced EMI principles. This design has been optimized specifically for meeting the increased standoff requirements for underwater towed operation. Our electromagnetic analysis results demonstrate that the dynamic classification methods used on land are applicable to underwater operations and can achieve high quality classification at the increased standoff range. Our hydrodynamic analysis results demonstrate that the 3D transmitter configuration provides a hydrodynamically stable design due to the increased metacentric height. Drag forces will not be significant or prohibitive for towed operation at the targeted survey speed (2-4 knots). Overall target localization error can be minimized (i.e., ~0.5m or less) through accurate measurement of the towline depth and line length.

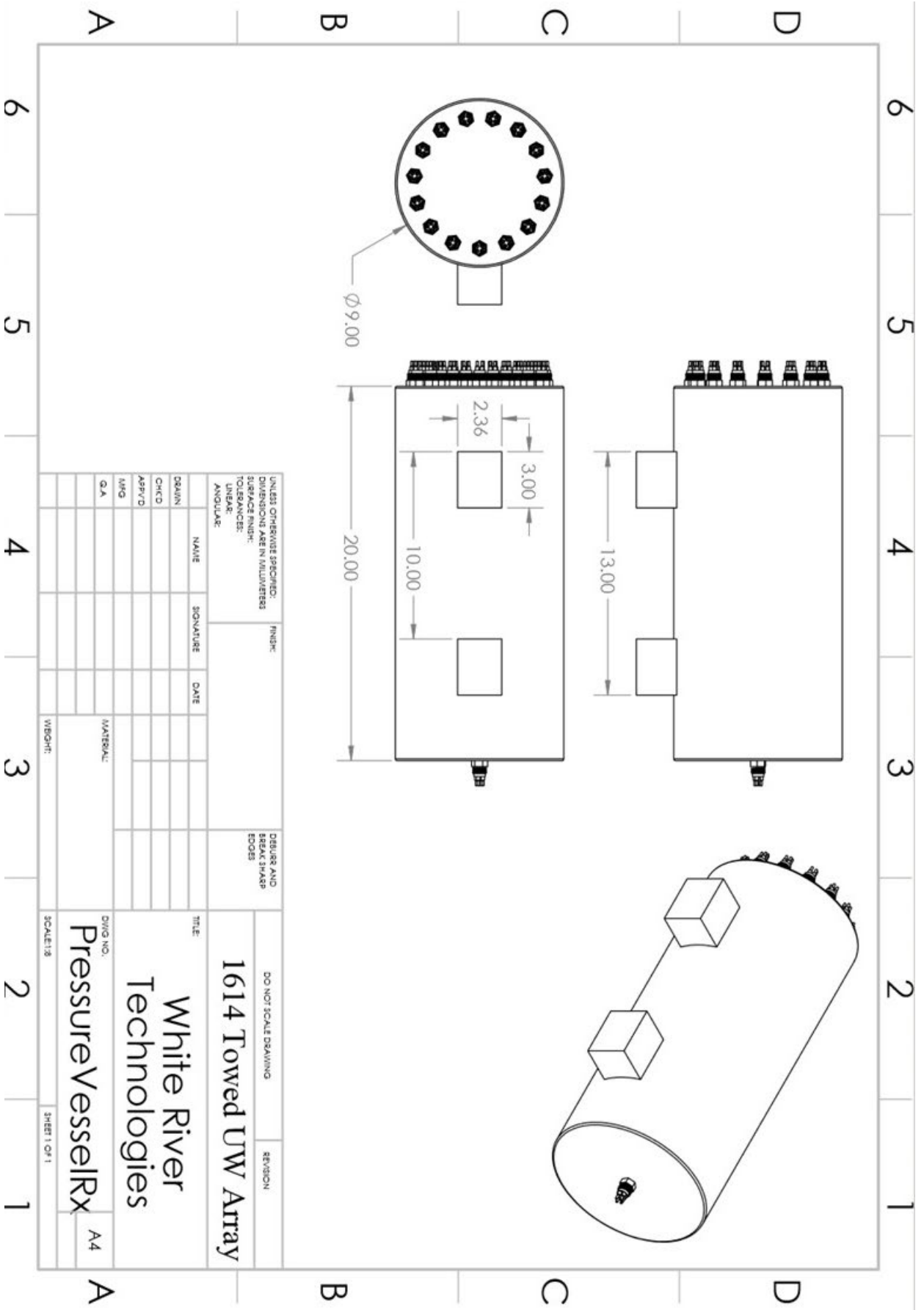
8.0 REFERENCES

- AETC Incorporated, 2005, "Marine Towed Array Technology Demonstration at the Former Naval Duck Target Facility", ESTCP Project 200324 Final Project Report
- Bell, T., Barrow, B., Steinhurst, D., Harbaugh, G., Friedrichs, C., and Massey, G., "Empirical Investigation of the Factors Influencing Marine Applications of EMI: Tank Testing," Interim Report, SERDP Project MR-2409, April 2016
- Billings, S., Song, L.P., "Determining Detection and Classification Potential of Munitions using Advanced EMI Sensors in the Underwater Environment", SERDP Project MR-2412 Final Report, November 2016
- Blevins, Applied Fluid Dynamics Handbook. Krieger Publishing House, 1984.
- Edwards, R.N., and Cheesman, S.J. (1987). Two-dimensional modelling of a towed transient magnetic dipole- dipole sea floor EM system. *Journal of Geophysics - Zeitschrift für Geophysik*. 61. 110-121.
- Environmental Security Technology Certification Program (ESTCP), 2014, Classification demonstration at the former Spencer Artillery Range, TN open area: ESTCP Summary Report, January 2014
- Funk, R., Feldpausch, R., Bridge, B., 2011, "Wide Area Assessment for Marine Munitions and Explosives of Concern", ESTCP Project MR-200808 Final Report
- Hill, S., Lombardo, L., and Fling, R., 2014, Standardized UXO technology demonstration site scoring record NO. 944, U.S. Army Aberdeen Test Center Report
- McDonald, J., 2008, "UXO Detection and Characterization in the Marine Environment", ESTCP Project MM-0324 Final Report
- Miller, J., 2017, "Detection and Discrimination in One-Pass Using the OPTEMA Towed-Array", ESTCP Project MR-201225 Final Report
- Morrison, F., 2014, "Development and Testing of an Engineering Prototype for a Marine Version of the Berkeley Unexploded Ordnance Discriminator (BUD): Phase II", SERDP Project MR-2321 Final Report
- Schultz, G., Keranen, J., Billings, S., Foley, J., Fonda, R., Hodgson, J., 2011, "Integrated Methods for Marine Munitions Site Characterization: Technical Approaches and Recent Site Investigations", *Marine Technology Society Journal*, Vol. 45, No. 6, pp. 47-61

Steigerwalt, R., Trembanis, A., Tait, G., Schmidt, V., Junck, B., 2014, "Autonomous Underwater Vehicle Munitions and Explosives of Concern Detection System", ESTCP Project MR-201002 Demonstration Report

Swidinsky, A., and Nabighian, M. N., 2016: Transient electromagnetic fields of a buried horizontal magnetic dipole. *Geophysics*, 81(6), E97-E110





UNLESS OTHERWISE SPECIFIED: DIMENSIONS ARE IN MILLIMETERS TOLERANCES: LINEAR: ANGULAR:			FINISH:	DEBUR AND BREAK SHARP EDGES	DO NOT SCALE DRAWING	REVISION
DRAWN	NAME	SIGNATURE	DATE	TITLE	1614 Towed UW Array	
CHKD				White River Technologies		
APP'D				Pressure Vessel Rx		
MFG				DWG NO.	A4	
G.A.				MATERIAL:	A4	
				WEIGHT:	SHEET 1 OF 1	